NASA Technical Memorandum 103909

Intersecting Shock-Wave/ Turbulent Boundary-Layer Interactions at Mach 8.3

M. I. Kussoy and K. C. Horstman

February 1992

National Aeronautics and Space Administration

NASA Technical Memorandum 103909

Intersecting Shock-Wave/ Turbulent Boundary-Layer Interactions at Mach 8.3

M. I. Kussoy and K. C. Horstman, Eloret Institute, Palo Alto, California

February 1992

National Aeronautics and
Space Administration

Ames Research Center
Moffett Field, California 94035-1000

Intersecting Shock-Wave/Turbulent Boundary-Layer Interactions at Mach 8.3

M. I. KUSSOY* AND K. C. HORSTMAN*

Ames Research Center

Summary

Experimental data for two three-dimensional intersecting shock-wave/turbulent boundary-layer interaction flows at Mach 8.3 are presented. The test bodies, composed of two sharp fins fastened to a flat-plate test bed, were designed to generate flows with varying degrees of pressure gradient, boundary-layer separation, and turning angle. The data include surface pressure and heat transfer distributions as well as mean flow-field surveys both in the undisturbed and interaction regimes. The data are presented in a convenient form to be used to validate existing or future computational models of these hypersonic flows. The data are also on a 3.5-inch diskette included with this document, and are available through E-mail. This work was supported by a grant from NASA to Eloret Institute (NCC2-452).

Nomenclature

c_f	skin friction coefficient
C_h	heat transfer coefficient
M	Mach number
p,P	pressure
PT2	pitot pressure
PT2 INF	local free-stream pitot pressure ahead of interaction
P INF	local free-stream static pressure ahead of interaction
q,Q	heat flux
Q INF	heat flux ahead of interaction
Re	Reynolds number
RHO	density
RHO INF	local free-stream density ahead of interaction
RHOU	mass flux (ρu)
RHOU INF	local free-stream mass flux ahead of interaction
s,S	distance along fin surface measured from leading edge
T	temperature
T INF	local free-stream static temperature ahead of interaction
TT	stagnation temperature
TT INF	local free-stream temperature ahead of interaction
u,U	total velocity
U INF	local free-stream velocity ahead of interaction
x,X	streamwise coordinate, distance from leading edge of sharp fin
y,Y	distance normal to flat-plate model surface
z,Z	spanwise distance measured from symmetry line of test geometry
α	yaw or fin angle
δ	boundary-layer thickness
δ^*	compressible displacement thickness
θ	compressible momentum thickness
ρ	density
τ	shear stress

Subscripts

avg	average value
i	initial value
0	initial conditions
T	wind-tunnel stagnation conditions
w	wall
∞	local free-stream ahead of interaction

*Eloret Institute, Palo Alto, California.

Introduction

To design realistic aerodynamic vehicles to fly in the hypersonic flow regime, it is of primary importance to have the ability to predict, with reasonable reliability, the aerodynamic characteristics of such vehicles. Only in this manner can long and expensive design programs be successful as efficient designs are identified and studied. However, before one attempts to predict the aerodynamics of the flow over a complex vehicle (with a cockpit, fuel tanks, and other appurtenant structures), one should be able to reliably predict basic flow properties (such as surface pressures, heat transfer distributions, skin friction lines, extent of separation, flow direction, etc.) on simple generic shapes. Without verification of computations with experimental measurements on a simple body, any a priori prediction of the flow field over a complex body could be in gross error.

One of the key elements in any air-breathing hypersonic vehicle is the inlet. This device, usually composed of two or more vertical surfaces attached to the vehicle's exterior and covered by a cowl, is normally located in a far downstream position at the end of a ramp. We have identified several key elements of a generic hypersonic inlet: a thick turbulent boundary-layer approaching two vertical fins, a crossing shock pattern, vortices, large pressure gradients, and separation zones. An experiment was designed which focused on these salient features of a generic hypersonic inlet. The basic configuration consisted of a pair of sharp vertical fins attached to a flat plate test bed. The approaching undisturbed equilibrium fully developed hypersonic turbulent boundary-layer (which which was verified by detailed boundary-layer surveys) occupied a significant portion of the open inlet area. The fin spacing geometry was determined as that which would allow the two primary shocks to intersect without any weakening from the expansion fans off the fin corner.

Two pairs of fins were tested, with compression angles of 10° and 15° respectively, in order to observe the effect of different shock strengths on the entire flow field. This paper presents experimental data obtained using these test models. The data obtained during this test program (undisturbed flow field surveys, surface pressure and heat transfer distributions, and extensive flow-field surveys for the two inlet configurations) can be used as a data base against which existing computer codes should be verified. In this way, turbulent flow models can be evaluated against relatively simple three-dimensional (3-D) flows in which the basic characteristics of a more complex flow over a real vehicle are present.

The authors owe a large debt of gratitude to NASA Ames Research Center 3.5-Foot Hypersonic Wind Tunnel personnel, namely mechanical test technicians Mike Reeves (shift leader), Robert Finnie, and Reuben Torrecampo; and electronic technician Ismael "Bong" De La Cruz. Without their efforts during this investigation, the present results, obtained during a relatively short tunnel entry, would not have been possible.

Description of Experiment

Facility

The experiment was conducted in the Ames 3.5-Foot Hypersonic Wind Tunnel Facility where heated high-pressure air flows through a 1.067-m diameter test section to four low-pressure spheres. The tunnel is of the open-jet design, which allows models to remain outside the stream until the required flow conditions are established. Models are rapidly inserted, and just as rapidly retracted prior to tunnel shutdown. Damage to models and instrumentation are thus held to a minimum. The nominal free-stream test conditions were: wall temperature ratio $T_w/T_0 = 0.27$, free-stream unit Reynolds number = 5.3×10^6/m, and free-stream Mach number = 8.28. The test core diameter was approximately 0.6 m. Useful test time was 3 min. Run-to-run variations in tunnel total pressure were less than 0.5%. However, the wind tunnel total temperature varied up to 50 K from run to run and, in addition, during a single run it varied about 90 K over the 3-min test time. These variations required special heat transfer data reduction procedures which will be discussed later.

Test Bodies

Basic test bed– The test bed consisted of a sharp flat plate, 76 cm wide, 220 cm long, and 10 cm thick (see fig. 1). The plate was pitched at a –2° angle of attack to increase the test Reynolds number and provide a uniform two-dimensional flow field on the plate. The turbulent boundary-layer thickness at the downstream end of the test bed was approximately 4 cm. The leading edge of the plate consisted of a 10° invar wedge. The bed was of a hollow frame construction, with interchangeable access panels (76 cm wide, 25.4 cm long, and 0.6 cm thick) covering the upper and lower surfaces. The entire test bed was water cooled, maintaining a constant surface temperature of 300 ± 5 K during a run. (Cooling was turned off during heat transfer runs.) Several of the interchangeable access panels had 20 cm diameter holes in the center which would accommodate several different instrumentation ports. One port was instrumented with a series of pressure taps and two types of heat transfer gauges. Another port, uninstrumented, accommodated a

computer-controlled survey mechanism to which static pressure, total pressure, flow direction (yaw), and total temperature probes could be attached for flow field surveys.

Double fins– The fin pairs were placed on the test bed as shown in figure 1. Two geometries were tested—one pair had compression angles of 10° and the other 15°, designated as the 10 × 10 degree and 15 × 15 degree shock generators, respectively. The separation between the vertical sides was 15.2 cm at the fin leading edge, and 4.3 cm in the channel at the rear. These dimensions remained constant for the entire test series. The fin pairs could be easily moved between runs in the x or z direction by means of slotted "L" brackets attached to the fins and a slotted piece attached to the flat plate surface. This arrangement is shown in figure 2. To obtain continuous data throughout the interaction region, the fin pairs were moved in the streamwise direction while the instrumentation port remain fixed. The undisturbed boundary-layer thickness at the incident shock-wave impingement point increased about 10% in a distance corresponding to the difference between the farthest upstream and downstream positions of the fins. However, this had little effect on the experimental results provided they were compared at an equivalent distance from the fin leading edge. The fin leading edges were located on the flat plate at an average distance of about 163 cm from the flat-plate leading edge. Each fin was 40 cm long and 20 cm high.

Instrumentation

One instrumented port was used in this investigation. This port, used on the test bed, was 20 cm in diameter and had rows of parallel pressure taps, thermocouples, and Schmidt-Boelter heat transfer gauges which ran close to and on either side of the center line. This port had a series of mounting holes along the edge, and could be oriented in any direction with respect to the oncoming undisturbed flow.

Surface Pressure

The surface static pressure taps were 0.16 cm in diameter, connected with short lengths of stainless steel tubing (10 to 15 cm long) to individual strain gauge differential-pressure transducers (PSI brand). These pressure cells were all located in a small self-contained modular unit, which had a built-in pressure scanning system (electrical, not mechanical). This system was designed to be calibrated in situ with carefully monitored pressures. The calibrations were made by varying the pressure on the reference side of the cell, and recording it using a Datametric strain-gauge differential pressure cell which itself had been calibrated previously with a dead-weight tester. Calibrations were made immediately prior to each run and were linear and repeatable to within 1%. The modular unit containing the transducers was located within the test bed and was water-cooled. The complex flow fields investigated herein usually encompass a wide pressure range. To obtain the highest accuracy, three pressure modules were used. One, with a range of ±1 psia, was used to obtain accurate measurements of the free-stream static pressure (of the order of 0.062 psia) as well as the other low static pressures present on the model surface and in the flow field. The other pressure modules had ranges of ±5 and ±45 psia.

Surface Heat Transfer

Surface heat transfer was obtained using two techniques—the transient thin-skin method, and a measurement using a thermopile. The transient thin-skin method utilized chromel-constantan thermocouples spot-welded approximately 1 cm apart to the interior surface of the instrumentation ports. The port thickness was approximately 0.025 cm at that point. For these tests, the entire model was kept at room temperature, then inserted into the flow after the desired flow conditions were obtained. Depending on the thermocouple location, the temperature rise (with the internal model water-cooling disconnected) varied from 10 to 70 K during a typical 5- to 10-second heat transfer run. Measurements of T_T and T_w were taken twice per second during the run. The data were reduced by obtaining a least squares linear fit of $\ln [(T_T - T_w)/(T_T - T_{wi})]$ versus time. This accounted for any small variations in tunnel total temperature during these 5 to 10 seconds (about 20 to 30 K). Calculations, using the procedures outlined in reference 1, indicated that for the present test conditions the interior wall temperature follows the exterior wall temperature after 2 seconds and that longitudinal conduction errors are less than 5% of the measured convective heat transfer. Therefore, these corrections were not applied to the data.

Heat transfer rates were also measured using miniature Schmidt-Boelter heat transfer gauges. These gauges, 0.20 cm diameter by 0.6 cm long, consisted of a thermopile to measure the temperature difference across a known substrate located just below the surface. A factory calibration was used to relate the gauge output (in millivolts) to the heat transfer rate, q. Two calibrations were used, one with a range of q from 0 to 3 Btu/ft^2 sec and the other with a range of 3 to 30 Btu/ft^2 sec, to obtain the highest measurement accuracy over the entire range of measurements. These calibrations had to be modified after several runs, since the harsh environment during a run affected the gauges' performance. These gauges are

essentially steady state devices, giving a stable reading after about a second or two. They were placed 1.8 cm apart. Although the data reduction procedure for the Schmidt-Boelter gauges is simpler than the thin-skin method, the results from the thin-skin method are more consistent and believed to be more reliable than the results from the Schmidt-Boelter gauges.

Parallel rows of thermocouples and Schmidt-Boelter gauges were placed in the flat-plate instrumentation port, and these data (along with surface pressures) were recorded simultaneously during a run.

The surface heat transfer results were not corrected for the small longitudinal conduction errors (less than 5%) but were corrected for run-to-run variations in wind tunnel total temperature (less than 50 K). This was done by assuming that the heat flux divided by the driving potential ($T_T - T_w$) is invariant for small changes in total temperature. Therefore, q(corrected) = q(measured) × $[(T_{Tavg} - T_w)_{nominal}/(T_{Tavg} - T_{wi})_{measured}]$. Changes in wind tunnel total temperature during a 5- to 10-second heat transfer run were typically less than 25 K, and the changes were very consistent from run to run. Thus an average value of total temperature over the run time was used for each run.

Survey Mechanism

Flow field surveys were obtained with the computer-controlled survey mechanism located within the model. This mechanism was designed to move a probe in two directions—vertical (Y) and yaw (α)—using individual motors. Precision anti-backlash gears were driven by stepping motors, whose shafts were capable of turning in small controlled increments. The vertical motion was accomplished by a rack and pinion gear combination. The resolution in yaw was 0.5°. The rotary motion of the motor shafts in both directions was coupled to anti-backlash bevel gears connected to multi-turn precision potentiometers.

Pitot Pressure Probe

Pitot pressures in the undisturbed flow field were measured by a stainless steel probe described in references 2 and 3. The probe was calibrated in a free-jet facility—matching Mach number, velocity, and density with the present test conditions. This calibration indicated that the errors due to rarefaction effects were less than 1%; therefore, no corrections were applied to the pitot data. This probe was attached to one port of the PSI module discussed above with a short length (about 8 cm) of stainless steel tubing. The pressure transducer calibration procedure was identical to the surface pressure procedure discussed previously.

Static Pressure Probe

Static pressures in the undisturbed flow field were measured by a stainless steel probe described in references 2 and 3. This probe is geometrically similar to the one used in reference 4, i.e., a 10° cone-cylinder. Independent calibrations to account for viscous interaction effects agreed with the calibration of Behrens (ref. 4). The viscous corrections applied to the data were up to 20%. The probe was attached to one port of the PSI module discussed above with a short length (about 8 cm) of stainless steel tubing. The pressure transducer calibration procedure was identical to the surface pressure procedure discussed previously.

Total Temperature Probe

Total temperatures in the undisturbed flow field were measured with the probe described in references 2 and 3. This probe was designed using a concept suggested by Vas (ref. 5). An unshielded, butt-welded chromel-alumel thermocouple (approximately 0.3 cm long and 0.013 cm thick) is supported by tapered chromel and alumel posts. A second chromel-alumel thermocouple is formed at the end of the alumel support. This provides a simultaneous temperature measurement of the butt-welded thermocouple junction and the probe support.

Corrections for radiation, conduction and recovery factor were made following the method of reference 5. To make these corrections, the local Mach number and Reynolds number must be known, requiring an iterative procedure using the pitot and static pressure data. Independent calibrations of these probes in the wind tunnel free stream indicated a maximum total temperature error of 2%.

Cobra Probe

In order to measure yaw angle and total pressure in the interacting flow field, a three-hole flow direction probe (cobra probe) was used. The diameter of the individual probe was 0.107 cm, and the overall width was three times that, or 0.32 cm. The characteristics of this probe, as well as some possible calibration techniques, are discussed in reference 6. These probes can, within limits recognized and defined from the calibration, be used in either of two basic modes. One mode is to null the probe, assuring that the pressures seen by the outer tubes are equal (taking into account the differing calibrations of the pressure transducers connected to each tube). Using this mode, a probe calibration (pressure vs. yaw for each tube)

is only necessary to determine an offset due to minute physical asymmetries in fabrication. The nulling procedure involves moving the probe to a Y location, waiting 3 or 4 sec for the outer tubes to give a steady reading, comparing these readings, determining which direction and how many degrees to rotate the probe, waiting again for a steady reading, comparing them again, etc. This is certainly feasible using our high speed data acquisition system (Schwartz); but, with less than a 3-min run time available, a complete survey with respectable resolution in Y and yaw angle would probably take two or three separate tunnel runs.

Alternatively, we decided that a more practical method would be to calibrate the probe in the undisturbed boundary-layer at several vertical positions (thus varying Mach number) for a range of yaw angles. This would provide us with the zero offset, interference effects (when close to the model surface), as well as limitations in Mach number and maximum usable yaw angle range. Following reference 6, a normalized pressure parameter, $(P_1 - P_3)/[P_2 - 0.5 * (P_1 - P_3)]$, could be computed, where the subscripts 1 and 3 indicate the two side pressure tubes and 2 the middle tube of the cobra probe. This parameter was plotted versus the yaw angle, and the data fitted with a cubic curve fit. The results of these calibrations showed that the probe calibration was independent of Mach number and thus usable for $Y > 0.2$ cm and $\pm 25°$ in yaw angle. With this technique the procedure was to fix the probe yaw angle and incrementally raise the probe through the boundary-layer.

Experimental Uncertainties

The uncertainties in the surface pressure were estimated to be $\pm 10\%$ or ± 80 N/m^2, whichever is larger. The uncertainties in the surface heat flux measurements were estimated to be $\pm 10\%$. For the flow-field quantities, the estimated uncertainties are $\pm 2\%$ for the total temperature, $\pm 10\%$ for the static pressure, $\pm 6\%$ for the static temperature, $\pm 12\%$ for the density, $\pm 3\%$ for the velocity, $\pm 3°$ for yaw angle, and $\pm 5\%$ for the pitot pressure. The uncertainty in Y is ± 0.02 cm. These uncertainties in the flow-field variables are due principally to zero offsets in the pressure and yaw angle measurements. Since each survey was obtained with a single probe, the uncertainty of the vertical variation in these flow-field quantities is significantly less than the numbers quoted above.

Experimental Results

The test data were obtained during a series of runs with the wind tunnel operating at the nominal conditions described above. Before each run, the test body was positioned outside of the open jet. Flow was then initiated. When the desired test conditions were reached, the model was inserted into the test stream. The model was retracted prior to tunnel shutdown.

Undisturbed Test Bed Results

To establish the presence of a fully developed equilibrium hypersonic turbulent boundary-layer approaching the interaction region, pitot pressure, static pressure, and total temperature surveys of the boundary-layer were taken at a distance of 162 cm from the flat-plate leading edge. For these undisturbed boundary-layer surveys, the flat-plate test body was run devoid of any fins. Velocity, density, and pressure profiles were obtained from the pitot and static pressure and total temperature surveys. Each survey was taken during a single test run. In traversing the flow field, the probe was stopped at each location for a few seconds to ensure no time lag in the pressure or temperature measurement. Survey data were obtained up to 4.0 cm from the flat-plate model surface. The static pressure at the model surface was monitored continuously during all traverses to verify that the data were free from interference effects. The data presented here have assumed a constant static pressure through the boundary layer. Actual measurements, after applying the viscous interaction correction, indicated a random variation of $\pm 5\%$. The velocity profiles obtained from these mean flow-field surveys were transformed into incompressible coordinates using the Van Driest II transformation (ref. 7) and are shown in figure 3 in law-of-the-wall coordinates. Also shown on this plot is Coles' universal law-of-the-wall (ref. 8). These profiles verify the presence of a hypersonic fully developed turbulent boundary-layer in the interaction region for the fin flows being investigated. Using the law-of-the-wall concept, surface skin friction can be determined; this value was $c_f = 0.99 \times 10^{-3}$. For any turbulence model verification procedure, these initial boundary-layer conditions should be verified (or set) by the computation. The measured local free-stream conditions are given in table 1. Quantities measured during the surveys, as well as derived quantities, are presented in table 2 for the undisturbed boundary-layer at $x = 162$ cm. For both double fin flows, the distance from the fin leading edge to the flat-plate leading edge varied from 152 to 174 cm (an average of about 163 cm). In reference 9, boundary-layer measurements were made on the same model, and similar free-stream conditions at $x = 187$ cm.

The flat-plate instrumentation port was aligned with its rows of instrumentation parallel to the flow direction and measurements were made from the most downstream to the most upstream positions on the flat plate that were

physically possible. The resulting longitudinal pressure and heat transfer distributions are reported in reference 9. The pressure was essentially constant, while the heat transfer decreased as x increased. It is speculated that the end of natural transition occurred at about 100 cm, although we have no direct measurements through the transition region. The flat-plate instrumentation port was also oriented perpendicular to the oncoming flow. These results indicated that both pressures and heat transfer rates were essentially constant over an 18-cm-wide, centrally located zone on the model surface both 165 and 190 cm back from the leading edge. (Variations in these data within this zone were within the experimental accuracy of the measurements.) Also, results from surface oil film studies showed a much wider area of surface skin friction lines parallel to the flat plate center line.

From the foregoing results, it was concluded that a two-dimensional boundary-layer existed, running parallel to the plate edges (observed from oil-flow visualization traces), with negligible longitudinal gradients, and becoming quite large (nearly 4 cm high) at the rearward stations where the interactive flow was initiated.

Double-Fin Interaction Results

The flat-plate instrumentation port was positioned, in separate runs, with either the row of pressure taps or thermocouples on the plane of symmetry. The resulting pressure and heat transfer distributions are shown in figures 4 and 5, respectively, and are tabulated in table 3. All transverse stations chosen for the two double-fin configurations are indicated on figures 4 and 5. The point of the double-shock intersection (from inviscid considerations only) is also shown on these figures. From a knowledge of the incoming Mach number, the x location close to where the two shock waves would most likely meet was chosen as one station for transverse (z direction) surface pressure measurements. The other x stations were chosen at positions near the maximum streamwise pressure, and at one location in the straight channel part of the geometry. Also for the 10 × 10 degree shock generator pair, one station chosen was about 9 cm upstream of the shock crossing location.

Oil flow visualization observations were made for each fin configuration on both the flat-plate and fin surfaces, using a thin mixture of machine oil and chalk dust. The oil would evaporate or flow downstream, leaving a thin trace of chalk dust on the surface, which could be lifted off (using special wide scotch tape) and permanently placed on a plain white sheet. Photos of these oil flows are shown in figures 6 through 9. Since the originals do not reproduce well, flow directions were traced from the original and are shown, in the same scale, in these figures as well.

For convenience, the transverse measuring stations, as well as the inviscid shock intersection location, are indicated on both photos and sketches in these figures. In figures 8 and 9, the longitudinal scale shown is x; the actual distance along the compression surface can be obtained from the fin geometry. Flat-plate surface flow angles were measured at these transverse stations, and are given in table 4. Surface pressures and heat transfer rates were measured on the adjacent flat-plate surface for both the 10° and 15° configurations at the previously mentioned transverse stations, and are also given in table 4. Two things should be noted concerning these transverse measurements. First, since the pressure taps, thermocouples, and Schmidt-Boelter gauges were displaced in x on the instrumentated port, a transverse measuring station (for example, x = 18.2 cm) will have three x values associated with it (for example, x = 18.2 cm for transverse wall pressures, x = 16.5 cm for heat transfer from thermocouples, and x = 19.5 cm for heat transfer from Schmidt-Boelter gauges). Second, even though these results were taken across the entire span, they are presented with z representing the distance from the centerline without regard to direction. The transverse wall pressures and transient thin-skin heat transfer results were symmetric about the centerline, within experimental accuracy.

Two sets of flow-field surveys were done, one for each of the configurations investigated. For both configurations, at each transverse station, the distance between the centerline (z = 0) and the fin surface was divided into four or five equal increments, and surveys were made, in the vertical (y) direction, at each of these equally spaced z increments. At each x,z location, two surveys were made; one with a "short" probe, which measured the pitot pressures and yaw angles from y values of 0.25 to about 3.45 cm, and the other with a "long" probe, which covered the vertical distance between 2.80 and 6.5 cm. These measurements were then merged, using the overlapping portion as a guide, and data reported from y = 0.25 to 6.0 cm. In the converging part of the geometry, the cobra probe axis was set to the fin angle (10° or 15°), and in the channel part it was set to point directly upstream. It was felt that fixing the probe at these angles would ensure that it would always be operating within its valid calibration range. Pitch was not measured, but it was felt that pitch angles of less than 10° (which would seem to be the case here) would not affect the yaw results. These vertical surveys were done in a manner similar to that described above for the single boundary-layer probes. After each survey, the fin pairs were then translated in the z direction a given distance (using the slot arrangement described above and shown in figure 2) with the x distance being kept constant, and another survey run. The data obtained from these flow-field

surveys, namely pitot pressures and yaw angles, are given in tables 5 and 6. These data are the results of averaging many data points at each y location taken during each individual survey. These individual vertical surveys at a given x location were processed to give contour plots of pitot pressure ratio and yaw angle. These plots are presented in figures 10 through 13.

Concluding Remarks

Two cases of an intersecting shock-wave/hypersonic turbulent boundary- layer interaction flow have been experimentally investigated. These particular cases were chosen because they were relatively simple, yet exhibited some of the basic flow characteristics of hypersonic inlets. Streamwise and transverse surface pressure and heat transfer distributions, as well as flow-field surveys which measured pitot pressures and yaw angles in the interaction regime, are presented. The tabulated results presented in this report provide, in sufficient detail, experimental data for validating numerical computations of turbulent complex flows.

References

1. George, A. R.; and Reinecke, W. G.: Conduction in Thin-Skinned Heat Transfer and Recovery Temperature Models, AIAA J., vol. 1, no. 8, Aug. 1963, pp. 1956-1958.

2. Kussoy, M. I.; and Horstman, C. C.: An Experimental Documentation of a Shock-Wave Turbulent Boundary-Layer Interaction Flow With and Without Separation. NASA TMX 62,412, February 1975.

3. Kussoy, M. I.; and Horstman, C. C.: Documentation of Two and Three-Dimensional Hypersonic Shock-Wave/Turbulent Boundary-Layer Interaction Flows. NASA TM-101075, January 1989.

4. Behrens, W.: Viscous Interaction Effects on a Static Pressure Probe at M = 6. AIAA J., vol. 1, no. 12, Dec. 1963, pp. 2864-2866.

5. Vas, I. E.: Flow Field Measurements Using a Total Temperature Probe at Hypersonic Speeds. AIAA J., vol. 10, no. 3, March 1972, pp. 317-323.

6. Dudzinski, Thomas J.; and Krause, Lloyd N.: Flow-Direction Measurement With Fixed-Position Probes. NASA TMX-1904, October 1969.

7. Van Driest, E. R.: The Problems of Aerodynamic Heating. Aerospace Engineering Review, 1956, pp. 26-41.

8. Coles, D. E.: The Turbulent Boundary Layer in a Compressible Fluid. Rand Corporation, Report R-403-PR, 1962.

9. Kussoy, M. I.; and Horstman, K. C.: Documentation of Two- and Three-Dimensional Shock-Wave/ Turbulent-Boundary-Layer Interaction Flows at Mach 8.2. NASA TM-103838, May, 1991.

Table 1. Free-stream conditions (x = 162 cm)

M_∞	= 8.28
T_∞	= 80 K
p_∞	= 430 N/m^2
ρ_∞	= 0.0186 kg/m^3
T_w	= 300 K
U_∞	= 1483 m/sec
δ_0	= 3.25 cm
δ_0^*	= 1.26 cm
θ_0	= 0.083 cm
τ_{w_∞}	= 21.6 N/m^2
q_{w_∞}	= 10400 W/m^2
Re_{δ_0}	= 1.7×10^5
Re_{θ_0}	= 4.4×10^3
Re/m	= 5.3×10^6
c_{f_∞}	= $\dfrac{\tau_{w_0}}{1/2\rho_\infty U_\infty^2} = 0.99 \times 10^{-3}$
C_{h_∞}	= $\dfrac{q_{w_\infty}}{\rho_\infty U_\infty (0.9T_T - T_w)} = 0.56 \times 10^{-3}$

Table 2. Upstream boundary layer

Y (cm)	M	P/ P INF	RHO/ RHO INF	T/ T INF	U/ U INF	RHOU/ RHOU INF	TT/ TT INF
0.000	0.000	1.000	0.267	3.744	0.000	0.000	0.270
0.110	2.330	1.000	0.243	4.109	0.571	0.139	0.609
0.210	3.252	1.000	0.290	3.445	0.730	0.212	0.753
0.320	3.530	1.000	0.318	3.148	0.758	0.241	0.770
0.420	3.772	1.000	0.338	2.957	0.785	0.265	0.795
0.520	4.058	1.000	0.356	2.811	0.823	0.293	0.840
0.620	4.297	1.000	0.380	2.631	0.843	0.320	0.859
0.720	4.550	1.000	0.406	2.464	0.864	0.351	0.879
0.820	4.703	1.000	0.423	2.362	0.874	0.370	0.889
0.930	5.076	1.000	0.490	2.043	0.877	0.430	0.873
1.030	5.247	1.000	0.499	2.002	0.898	0.448	0.902
1.130	5.477	1.000	0.526	1.903	0.914	0.480	0.921
1.240	5.678	1.000	0.559	1.789	0.919	0.514	0.921
1.340	5.891	1.000	0.582	1.718	0.934	0.544	0.942
1.440	6.039	1.000	0.600	1.666	0.943	0.566	0.953
1.540	6.259	1.000	0.628	1.591	0.955	0.600	0.968
1.640	6.371	1.000	0.636	1.572	0.966	0.614	0.986
1.750	6.571	1.000	0.670	1.492	0.971	0.651	0.989
1.850	6.765	1.000	0.700	1.429	0.978	0.685	0.997
1.950	7.005	1.000	0.746	1.341	0.981	0.732	0.996
2.050	7.171	1.000	0.783	1.278	0.980	0.767	0.991
2.150	7.373	1.000	0.817	1.224	0.987	0.806	0.998
2.250	7.492	1.000	0.843	1.186	0.987	0.832	0.996
2.350	7.647	1.000	0.869	1.150	0.992	0.862	1.003
2.450	7.800	1.000	0.901	1.110	0.994	0.896	1.004
2.550	7.875	1.000	0.918	1.090	0.994	0.912	1.003
2.650	7.949	1.000	0.936	1.068	0.994	0.930	1.001
2.750	8.023	1.000	0.944	1.059	0.999	0.943	1.009
2.850	8.074	1.000	0.941	1.063	1.007	0.948	1.023
2.940	8.132	1.000	0.960	1.042	1.004	0.964	1.017
3.030	8.189	1.000	0.962	1.039	1.010	0.972	1.027
3.120	8.233	1.000	0.988	1.012	1.002	0.990	1.011
3.220	8.275	1.000	0.999	1.001	1.001	1.000	1.009
3.310	8.275	1.000	1.009	0.991	0.996	1.005	1.000

Table 3. Streamwise centerline surface pressure and heat transfer distribution

10 × 10 degree shock generator Streamwise centerline surface pressures on flat plate			
X (cm)	P/P INF	X (cm)	P/P INF
0.20	0.85	22.35	5.24
1.20	0.84	23.35	5.73
2.20	0.82	24.35	6.19
3.19	0.85	25.34	6.87
4.19	0.82	26.34	7.52
5.22	0.90	27.37	8.27
6.20	0.86	28.35	8.85
7.20	0.88	29.35	9.55
8.20	0.89	30.35	10.31
9.20	1.01	31.35	11.48
10.20	1.16	32.35	13.23
11.20	1.43	33.35	14.97
12.19	1.69	34.34	14.92
13.19	2.05	35.34	13.48
14.19	2.42	36.34	11.92
15.19	2.92	37.34	10.66
16.19	3.23	38.34	9.52

10 × 10 degree shock generator Streamwise centerline surface heat transfer on flat plate from thermocouples			
X (cm)	Q/Q INF	X (cm)	Q/Q INF
4.03	1.02	22.50	3.21
5.01	1.00	23.48	3.48
6.02	1.02	24.49	3.79
7.00	0.99	25.47	4.04
7.96	1.01	26.43	4.47
8.95	1.01	27.42	4.94
9.95	0.98	28.42	5.21
10.96	0.91	29.43	5.59
12.98	1.09	31.45	6.38
13.98	1.39	32.45	7.21
14.98	1.73	33.45	8.02
17.24	2.34	35.71	7.33
17.99	2.37	36.46	6.48
18.99	2.61	37.46	5.84
20.03	2.74	38.50	5.28

Table 3. Concluded

15 × 15 degree shock generator Streamwise centerline surface pressures on flat plate			
X (cm)	P/P INF	X (cm)	P/P INF
0.25	1.09	23.58	20.16
1.25	1.07	24.50	17.90
2.25	1.05	24.58	17.74
3.24	1.09	25.50	15.45
4.24	1.03	25.58	14.63
5.27	1.15	26.50	13.44
6.25	1.19	26.57	12.40
7.25	1.45	27.49	11.87
8.25	1.81	27.57	10.69
9.25	2.29	28.49	10.92
11.25	3.81	28.60	9.89
12.24	4.69	29.49	11.45
13.24	5.50	29.58	11.10
14.24	6.08	30.49	13.73
15.24	6.85	30.58	14.13
15.50	6.90	31.49	16.29
16.24	7.74	31.58	16.61
16.50	7.85	32.58	17.26
17.50	9.27	33.58	16.61
18.49	11.40	34.58	15.65
19.49	13.66	35.57	14.79
20.52	16.11	36.57	14.19
21.50	18.71	37.57	14.03
22.50	21.13	38.57	14.39
23.50	20.32	39.57	15.42
Streamwise centerline surface heat transfer on flat plate from thermocouples			
X (cm)	Q/Q INF	X (cm)	Q/Q INF
2.00	0.74	15.99	4.72
2.98	0.87	16.96	5.20
3.99	0.78	16.97	5.16
4.97	0.75	17.93	6.22
5.93	0.78	18.00	6.36
6.92	0.74	18.92	7.63
7.92	0.58	19.92	8.90
8.93	0.59	20.93	10.28
10.95	1.76	22.95	12.09
11.95	2.60	23.95	11.69
12.95	3.42	24.95	10.28
14.00	4.02	27.21	7.14
14.98	4.38	27.96	6.31
15.21	4.60	28.96	6.14
15.96	4.68	30.00	6.88

Table 4. Transverse surface pressure, yaw angle, and heat transfer distribution

10 × 10 DEGREE SHOCK GENERATOR TRANSVERSE SURFACE QUANTITIES, STATION 1			
Pressures (X = 18.2 cm)			
Z (cm)	P/P INF	Z (cm)	P/P INF
0.32	3.56	2.40	2.74
0.41	3.76	2.60	2.85
0.62	3.40	2.70	2.69
0.71	3.68	3.30	3.58
1.30	3.05	3.40	3.37
1.41	3.31	3.60	3.73
1.60	2.87	3.70	3.58
1.71	3.18	4.40	3.76
2.30	2.65		
Surface streamline angles (X = 18.2 cm)			
Z (cm)	α (deg)	Z (cm)	α (deg)
0.88	–7	2.65	29
0.88	–12	2.65	39
1.76	1	3.52	23
1.76	1	3.52	24
Heat transfer from thermocouples (X = 16.5 cm)			
Z (cm)	Q/Q INF	Z (cm)	Q/Q INF
0.22	1.95	2.23	1.89
0.47	1.98	2.41	1.63
0.52	1.67	2.53	2.18
0.77	1.92	2.71	1.90
1.22	1.25	3.42	2.48
1.43	1.45	3.72	2.80
1.52	1.42	4.40	2.60
1.73	1.28		
Heat transfer from Schmidt-Boelter gauges (X = 19.5 cm)			
Z (cm)	Q/Q INF	Z (cm)	Q/Q INF
0.60	1.63	2.40	2.35
0.90	1.89	2.70	2.19
0.90	1.53	2.70	2.94
1.20	1.57	3.00	2.35
10 × 10 DEGREE SHOCK GENERATOR TRANSVERSE SURFACE QUANTITIES, STATION 2			
Pressures (X = 26.0 cm)			
Z (cm)	P/P INF	Z (cm)	P/P INF
0.02	7.02	1.65	5.68
0.35	7.00	1.98	5.29
0.65	6.55	2.02	5.85
0.98	6.13	2.35	5.39
1.02	6.69	2.65	4.66
1.35	6.29	3.00	4.90
Surface streamline angles (X = 26.0 cm)			
Z (cm)	α (deg)	Z (cm)	α (deg)
0.75	6	1.50	4
0.75	0	2.25	14
1.50	12	2.25	3

Table 4. Continued

Heat transfer from thermocouples (X = 24.3 cm)			
Z (cm)	Q/Q INF	Z (cm)	Q/Q INF
0.60	3.34	1.93	3.55
0.93	3.32	2.10	3.75
1.09	3.68	2.43	3.46
1.42	3.60	2.60	3.28
1.60	3.29	3.10	2.49
Heat transfer from Schmidt-Boelter gauges (X = 27.3 cm)			
Z (cm)	Q/Q INF	Z (cm)	Q/Q INF
0.55	3.56	2.35	3.67
0.88	3.96	2.68	2.48
0.92	4.43	2.72	3.39
1.25	4.28		
10 × 10 DEGREE SHOCK GENERATOR TRANSVERSE SURFACE QUANTITIES, STATION 3			
Pressures (X = 34.0 cm)			
Z (cm)	P/P INF	Z (cm)	P/P INF
0.00	14.29	1.09	7.63
0.09	13.56	1.41	7.47
0.41	13.34	1.59	7.29
0.59	12.74	1.91	6.98
0.91	12.94	2.00	6.65
1.00	10.00	2.00	6.82
1.00	9.45	2.07	4.50
Surface streamline angles (X = 34.0 cm)			
Z (cm)	α (deg)	Z (cm)	α (deg)
0.55	–24	1.10	–9
0.55	–20	1.60	–14
1.10	–12	1.60	–7
Heat transfer from thermocouples (X = 32.3 cm)			
Z (cm)	Q/Q INF	Z (cm)	Q/Q INF
0.16	7.18	1.49	7.17
0.48	7.76	1.54	6.91
0.95	7.59	1.86	6.29
1.07	7.44	1.95	3.76
1.17	6.55		
Heat transfer from Schmidt-Boelter gauges (X = 35.3 cm)			
Z (cm)	Q/Q INF	Z (cm)	Q/Q INF
0.01	6.47	1.49	5.04
0.31	6.53	1.79	3.18
0.80	6.43	1.81	5.25
1.00	6.70		
10 × 10 DEGREE SHOCK GENERATOR TRANSVERSE SURFACE QUANTITIES, STATION 4			
Pressures (X = 38.3 cm)			
Z (cm)	P/P INF	Z (cm)	P/P INF
0.35	8.90	1.35	11.03
0.65	9.82	1.65	12.97
0.90	10.03	1.90	12.79
1.00	8.79	2.10	15.15
1.10	11.00		

Table 4. Continued

Surface streamline angles (X = 38.3 cm)			
Z (cm)	α (deg)	Z (cm)	α (deg)
0.55	5	1.10	0
0.55	4	1.60	–5
1.10	1	1.60	–2
Heat transfer from thermocouples (X = 36.6 cm)			
Z (cm)	Q/Q INF	Z (cm)	Q/Q INF
0.60	7.62	1.60	6.12
0.97	8.19	1.98	5.44
1.05	8.31	2.05	5.52
1.42	6.56		
Heat transfer from Schmidt-Boelter gauges (X = 39.6 cm)			
Z (cm)	Q/Q INF	Z (cm)	Q/Q INF
0.55	4.62	1.00	5.60
0.80	5.13	1.25	6.35
15 × 15 DEGREE SHOCK GENERATOR TRANSVERSE SURFACE QUANTITIES, STATION 1			
Pressures (X = 18.2 cm)			
Z (cm)	P/P INF	Z (cm)	P/P INF
0.16	10.52	1.60	7.87
0.39	10.81	1.85	8.19
0.61	10.26	2.15	7.15
0.87	9.89	2.40	6.73
1.16	8.74	2.60	6.71
1.42	9.27		
Surface streamline angles (X = 18.2 cm)			
Z (cm)	α (deg)	Z (cm)	α (deg)
0.53	–1	1.59	14
0.53	–7	1.59	8
1.06	7	2.12	19
1.06	2	2.12	19
Heat transfer from thermocouples (X = 16.5 cm)			
Z (cm)	Q/Q INF	Z (cm)	Q/Q INF
0.19	4.69	1.63	3.91
0.63	4.53	1.75	3.17
0.77	4.00	2.18	5.51
1.18	3.58	2.30	4.52
1.32	3.43	2.76	5.02
1.36	4.91		
Heat transfer from Schmidt-Boelter gauges (X = 19.5 cm)			
Z (cm)	Q/Q INF	Z (cm)	Q/Q INF
0.01	4.92	1.79	4.02
0.54	6.01	1.81	4.66
1.26	5.88		

Table 4. Concluded

15 × 15 DEGREE SHOCK GENERATOR TRANSVERSE SURFACE QUANTITIES, STATION 2			
Pressures (X = 22.5 cm)			
Z (cm)	P/P INF	Z (cm)	P/P INF
0.11	21.29	1.40	8.24
0.40	19.84	1.61	8.79
0.63	19.68	1.93	6.81
0.92	13.42	2.09	7.84
1.09	13.45		
Surface streamline angles (X = 22.5 cm)			
Z (cm)	α (deg)	Z (cm)	α (deg)
0.50	–7	1.05	–23
0.50	–11	1.59	–20
1.05	–20	1.59	–20
Heat transfer from thermocouples (X = 20.8 cm)			
Z (cm)	Q/Q INF	Z (cm)	Q/Q INF
0.01	9.93	1.42	7.68
0.46	9.65	1.53	8.85
0.53	9.88	1.94	4.54
0.98	9.21	2.02	6.27
1.01	9.82		
Heat transfer from Schmidt-Boelter gauges (X = 23.8 cm)			
Z (cm)	Q/Q INF	Z (cm)	Q/Q INF
0.39	8.09	0.91	7.19
0.89	6.67	1.41	5.57
15 × 15 DEGREE SHOCK GENERATOR TRANSVERSE SURFACE QUANTITIES, STATION 3			
Pressures (X = 27.0 cm)			
Z (cm)	P/P INF	Z (cm)	P/P INF
0.11	11.60	1.09	13.98
0.40	12.19	1.40	17.26
0.63	12.24	1.61	18.87
0.92	13.85	1.93	21.94
Surface streamline angles (X = 27.0 cm)			
Z (cm)	α (deg)	Z (cm)	α (deg)
0.50	0	1.05	2
0.50	–1	1.59	6
1.05	1	1.59	4
Heat transfer from thermocouples (X = 25.3 cm)			
Z (cm)	Q/Q INF	Z (cm)	Q/Q INF
0.01	10.03	1.42	10.00
0.46	10.35	1.53	10.74
0.53	10.74	1.94	7.31
0.98	11.16	2.02	8.40
1.01	11.47		
Heat transfer from Schmidt-Boelter gauges (X = 28.3 cm)			
Z (cm)	Q/Q INF	Z (cm)	Q/Q INF
0.39	4.60	0.91	5.96
0.89	5.90	1.41	8.74

Table 5. Flow-field pitot pressures

10 × 10 DEGREE SHOCK GENERATOR, STATION 1 (X = 18.2 cm)						
		PT2/PT2 INF				
Y (cm)	Z (cm) =	3.52	2.64	1.76	0.88	0.00
0.25		0.60	0.45	0.35	0.15	0.15
0.50		0.70	0.45	0.35	0.25	0.20
0.75		0.75	0.45	0.30	0.25	0.20
1.00		0.80	0.50	0.30	0.30	0.25
1.25		0.90	0.55	0.40	0.35	0.35
1.50		0.95	0.65	0.50	0.45	0.45
1.75		1.10	0.75	0.60	0.60	0.60
2.00		1.30	0.90	0.80	0.80	0.80
2.25		1.50	1.10	1.00	1.00	1.05
2.50		1.75	1.35	1.20	1.15	1.15
2.75		1.90	1.55	1.30	1.15	1.15
3.00		2.15	1.85	1.35	1.05	1.00
3.25		2.35	2.15	1.30	0.95	0.95
3.50		2.50	2.40	1.10	0.95	0.95
3.75		2.60	2.60	1.05	0.95	0.95
4.00		2.70	2.65	1.05	1.00	0.95
4.25		2.75	2.70	1.00	1.00	1.00
4.50		2.75	2.75	1.00	1.00	1.00
4.75		2.75	2.75	1.00	1.00	1.00
5.00		2.75	2.75	1.00	1.00	1.00
5.25		2.75	2.75	1.00	1.00	1.00
5.50		2.75	2.75	1.00	1.00	1.00
5.75		2.75	2.75	1.00	1.00	1.00
6.00		2.75	2.75	1.00	1.00	1.00

Table 5. Continued

10 × 10 DEGREE SHOCK GENERATOR, STATION 2 (X = 26.0 cm)					
		PT2/PT2 INF			
Y (cm)	Z (cm) =	2.25	1.50	0.75	0.00
0.25		0.85	0.85	0.50	0.30
0.50		1.25	1.00	0.65	0.40
0.75		1.40	0.90	0.65	0.50
1.00		1.55	0.85	0.60	0.45
1.25		1.60	0.85	0.50	0.40
1.50		1.70	0.85	0.45	0.35
1.75		1.85	0.90	0.40	0.35
2.00		2.00	1.05	0.45	0.40
2.25		2.15	1.25	0.55	0.40
2.50		2.30	1.50	0.75	0.50
2.75		2.40	1.85	1.00	0.75
3.00		2.45	2.25	1.45	1.10
3.25		2.50	2.70	1.95	1.50
3.50		2.55	2.75	2.65	1.90
3.75		2.60	2.75	3.05	2.50
4.00		2.70	2.75	3.20	3.10
4.25		2.75	2.75	3.15	3.50
4.50		2.75	2.75	3.00	3.50
4.75		2.75	2.75	2.85	3.00
5.00		2.75	2.75	2.80	2.55
5.25		2.75	2.75	2.75	2.20
5.50		2.75	2.75	2.75	1.85
5.75		2.75	2.75	2.75	1.60
6.00		2.75	2.75	2.75	1.40

Table 5. Continued

10 × 10 DEGREE SHOCK GENERATOR, STATION 3 (X = 34.0 cm)					
		PT2/PT2 INF			
Y (cm)	Z (cm) =	1.60	1.05	0.55	0.00
0.25		1.00	1.50	1.40	1.05
0.50		1.30	1.75	1.60	1.40
0.75		1.60	1.70	1.55	1.40
1.00		1.75	1.65	1.40	1.35
1.25		1.80	1.60	1.25	1.25
1.50		1.85	1.55	1.15	1.10
1.75		1.90	1.60	1.05	1.00
2.00		2.00	1.65	1.00	0.90
2.25		2.10	1.80	1.00	0.85
2.50		2.25	2.05	1.10	0.90
2.75		2.40	2.35	1.25	1.05
3.00		2.75	2.85	1.65	1.45
3.25		3.05	3.65	2.30	2.10
3.50		3.20	4.50	3.10	3.00
3.75		3.30	5.00	3.95	3.75
4.00		3.40	5.25	4.60	4.35
4.25		3.60	5.60	5.00	4.95
4.50		3.80	5.80	5.25	5.20
4.75		4.05	6.05	5.40	5.35
5.00		4.25	6.10	5.55	5.50
5.25		4.40	6.10	5.60	5.65
5.50		4.55	6.10	5.80	5.75
5.75		4.70	6.10	5.90	5.90
6.00		4.75	6.10	6.00	6.00

Table 5. Continued

10 × 10 DEGREE SHOCK GENERATOR, STATION 4 (X = 38.4 cm)					
		PT2/PT2 INF			
Y (cm)	Z (cm) =	1.60	1.05	0.55	0.00
0.25		1.65	1.55	1.20	1.00
0.50		1.90	1.75	1.25	1.15
0.75		2.15	1.60	1.20	1.15
1.00		2.25	1.45	1.10	1.10
1.25		2.25	1.25	1.00	1.00
1.50		2.15	1.10	0.90	0.95
1.75		2.05	1.00	0.85	0.90
2.00		2.00	1.00	0.85	0.85
2.25		1.95	1.00	0.85	0.85
2.50		2.00	1.10	0.90	0.90
2.75		2.10	1.30	1.10	1.15
3.00		2.35	1.60	1.50	1.60
3.25		2.70	2.00	2.15	2.40
3.50		3.00	2.45	2.80	3.25
3.75		3.15	3.10	3.60	4.00
4.00		3.25	3.50	4.15	4.40
4.25		3.35	3.75	4.30	4.55
4.50		3.40	3.80	4.40	4.60
4.75		3.45	3.85	4.50	4.65
5.00		3.45	3.85	4.55	4.65
5.25		3.50	3.80	4.60	4.60
5.50		3.50	3.75	4.65	4.50
5.75		3.50	3.90	4.65	4.50
6.00		3.50	4.00	4.70	4.50

Table 5. Continued

15 × 15 DEGREE SHOCK GENERATOR, STATION 1 (X = 18.2 cm)						
		PT2/T2 INF				
Y (cm)	Z (cm) =	2.12	1.59	1.06	0.53	0.00
0.25		1.40	1.20	0.85	0.40	0.25
0.50		1.50	1.10	0.85	0.60	0.35
0.75		1.55	1.00	0.65	0.55	0.45
1.00		1.60	0.95	0.50	0.50	0.40
1.25		1.75	1.00	0.45	0.45	0.40
1.50		1.90	1.15	0.50	0.35	0.35
1.75		2.05	1.30	0.55	0.35	0.30
2.00		2.25	1.60	0.75	0.40	0.35
2.25		2.40	1.95	1.05	0.55	0.45
2.50		2.55	2.40	1.50	0.80	0.70
2.75		2.65	2.70	2.20	1.25	1.10
3.00		2.80	2.90	2.70	1.90	1.65
3.25		2.90	3.05	3.10	2.75	2.10
3.50		2.95	3.10	3.25	3.50	2.20
3.75		3.05	3.20	3.30	3.60	2.15
4.00		3.15	3.25	3.35	3.45	2.00
4.25		3.20	3.25	3.40	3.35	1.70
4.50		3.20	3.30	3.45	3.35	1.45
4.75		3.20	3.30	3.45	3.30	1.20
5.00		3.25	3.30	3.50	3.30	1.05
5.25		3.25	3.30	3.50	3.30	1.00
5.50		3.25	3.30	3.50	3.30	1.00
5.75		3.30	3.30	3.50	3.30	1.00
6.00		3.30	3.30	3.50	3.30	1.00

Table 5. Continued

15 × 15 DEGREE SHOCK GENERATOR, STATION 2 (X = 22.5 cm)					
		PT2/PT2 INF			
Y (cm)	Z (cm) =	1.57	1.05	0.50	0.00
0.25		1.55	1.85	1.40	0.95
0.50		1.70	1.80	1.50	1.35
0.75		1.55	1.70	1.25	1.25
1.00		1.60	1.60	1.10	1.10
1.25		1.70	1.60	1.00	0.95
1.50		1.85	1.70	0.90	0.85
1.75		1.95	1.85	0.85	0.80
2.00		2.10	2.15	0.85	0.70
2.25		2.20	2.65	0.90	0.70
2.50		2.30	3.10	1.10	0.75
2.75		2.35	3.50	1.50	1.00
3.00		2.35	3.85	2.50	1.80
3.25		2.35	4.30	3.30	2.75
3.50		2.30	4.70	4.75	3.85
3.75		2.20	5.05	5.85	5.30
4.00		2.05	5.50	6.40	6.00
4.25		1.95	7.00	6.75	6.40
4.50		1.90	7.15	7.15	7.00
4.75		1.90	7.15	7.45	7.35
5.00		1.90	7.10	7.75	7.45
5.25		1.85	5.90	8.00	7.55
5.50		1.75	4.50	7.90	7.55
5.75		1.60	3.80	7.85	7.55
6.00		1.55	3.30	7.80	7.55

Table 5. Concluded

15 × 15 DEGREE SHOCK GENERATOR, STATION 3 (X = 27.0 cm)					
		PT2/PT2 INF			
Y (cm)	Z (cm) =	1.57	1.05	0.50	0.00
0.25		2.10	1.70	1.30	1.25
0.50		2.15	1.65	1.35	1.35
0.75		1.90	1.45	1.25	1.20
1.00		1.70	1.25	1.15	1.10
1.25		1.60	1.15	1.05	1.00
1.50		1.50	1.10	0.95	0.90
1.75		1.50	1.05	0.90	0.85
2.00		1.60	1.10	0.90	0.85
2.25		1.75	1.20	0.95	0.90
2.50		1.95	1.50	1.20	1.15
2.75		2.25	1.85	1.60	1.65
3.00		2.55	2.35	2.20	2.15
3.25		2.80	3.05	2.80	2.80
3.50		3.05	3.60	3.35	3.40
3.75		3.20	4.25	3.80	3.65
4.00		3.35	4.55	4.00	3.80
4.25		3.50	4.60	4.05	3.85
4.50		3.60	4.55	4.10	3.90
4.75		3.65	4.55	4.10	3.95
5.00		3.70	4.65	4.15	4.00
5.25		3.75	4.80	4.25	4.10
5.50		3.75	4.90	4.35	4.25
5.75		3.85	4.95	4.45	4.40
6.00		4.00	5.00	4.55	4.45

Table 6. Flow-field yaw angles

10 × 10 DEGREE SHOCK GENERATOR, STATION 1 (X = 18.2 cm)					
		Yaw angle (deg)			
Y (cm)	Z (cm) =	3.52	2.64	1.76	0.88
0.25		16	20	26	11
0.50		15	18	17	19
0.75		14	15	11	11
1.00		13	12	4	3
1.25		12	9	0	–3
1.50		11	7	–1	–5
1.75		10	6	–2	–6
2.00		9	5	–2	–6
2.25		9	4	–2	–5
2.50		9	4	–1	–5
2.75		9	5	0	–4
3.00		9	6	1	–2
3.25		9	7	2	–1
3.50		9	9	2	–1
3.75		9	9	2	0
4.00		9	10	1	0
4.25		10	10	0	0
4.50		10	10	0	0
4.75		10	10	0	0
5.00		10	10	0	0
5.25		10	10	0	0
5.50		10	10	0	0
5.75		10	10	0	0
6.00		10	10	0	0

Table 6. Continued

10 × 10 DEGREE SHOCK GENERATOR, STATION 2 (X = 26.0 cm)				
		Yaw angle (deg)		
Y (cm)	Z (cm) =	2.25	1.50	0.75
0.25		10	16	22
0.50		11	15	16
0.75		11	14	12
1.00		11	12	8
1.25		11	11	6
1.50		10	10	4
1.75		9	8	4
2.00		9	7	4
2.25		8	7	4
2.50		8	6	3
2.75		8	6	3
3.00		8	6	2
3.25		9	6	3
3.50		9	7	3
3.75		10	7	4
4.00		10	8	6
4.25		10	9	7
4.50		10	9	8
4.75		10	10	9
5.00		10	10	9
5.25		10	10	10
5.50		10	10	10
5.75		10	10	10
6.00		10	10	10

Table 6. Continued

10 × 10 DEGREE SHOCK GENERATOR, STATION 3 (X = 34.0 cm)				
		Yaw angle (deg)		
Y (cm)	Z (cm) =	1.60	1.05	0.55
0.25		–3	4	11
0.50		–1	5	9
0.75		1	5	8
1.00		2	5	8
1.25		2	5	7
1.50		1	6	7
1.75		0	6	7
2.00		–1	6	8
2.25		–2	5	9
2.50		–2	5	11
2.75		–3	4	12
3.00		–3	2	10
3.25		–3	1	7
3.50		–3	1	5
3.75		–4	0	4
4.00		–4	0	3
4.25		–4	0	2
4.50		–4	0	1
4.75		–4	0	1
5.00		–3	0	0
5.25		–3	0	0
5.50		–3	0	0
5.75		–3	0	0
6.00		–3	0	0

Table 6. Continued

10 × 10 DEGREE SHOCK GENERATOR, STATION 4 (X = 38.4 cm)				
		Yaw angle (deg)		
Y (cm)	Z (cm) =	1.60	1.05	0.55
0.25		–3	2	6
0.50		–1	3	3
0.75		0	3	1
1.00		1	2	0
1.25		2	1	0
1.50		2	0	–1
1.75		2	–2	–2
2.00		2	–4	–2
2.25		1	–5	–2
2.50		0	–5	–2
2.75		0	–5	–3
3.00		0	–6	–4
3.25		0	–5	–4
3.50		0	–5	–4
3.75		1	–4	–4
4.00		1	–4	–4
4.25		0	–3	–3
4.50		–1	–3	–3
4.75		–1	–3	–3
5.00		–1	–3	–3
5.25		–2	–4	–3
5.50		–2	–4	–3
5.75		–3	–4	–3
6.00		–3	–4	–3

Table 6. Continued

15 × 15 DEGREE SHOCK GENERATOR, STATION 1 (X = 18.2 cm)					
		Yaw angle (deg)			
Y (cm)	Z (cm) =	2.12	1.59	1.06	0.53
0.25		15	19	26	29
0.50		14	17	18	23
0.75		14	15	13	13
1.00		13	14	11	5
1.25		12	13	10	3
1.50		11	11	9	3
1.75		10	10	10	5
2.00		10	9	9	6
2.25		9	8	8	7
2.50		9	7	6	6
2.75		10	7	5	5
3.00		11	8	5	5
3.25		12	9	6	6
3.50		13	10	8	8
3.75		14	12	9	10
4.00		14	13	11	13
4.25		15	14	12	14
4.50		15	14	13	15
4.75		15	15	13	15
5.00		15	15	14	15
5.25		15	15	14	15
5.50		15	15	14	15
5.75		15	15	14	15
6.00		15	15	15	15

Table 6. Continued

15 × 15 DEGREE SHOCK GENERATOR, STATION 2 (X = 22.5 cm)				
		Yaw angle (deg)		
Y (cm)	Z (cm) =	1.57	1.05	0.50
0.25		0	4	16
0.50		1	3	7
0.75		0	3	1
1.00		–1	4	–3
1.25		–2	5	–4
1.50		–2	6	–2
1.75		–3	5	0
2.00		–3	4	4
2.25		–2	3	11
2.50		–2	2	16
2.75		–1	1	12
3.00		0	0	7
3.25		2	–1	4
3.50		4	–1	2
3.75		7	–2	1
4.00		10	–2	0
4.25		11	–3	0
4.50		10	–4	0
4.75		9	–5	–1
5.00		8	–5	–1
5.25		6	–6	–1
5.50		5	–7	–1
5.75		3	–8	–1
6.00		2	–9	0

Table 6. Concluded

15 × 15 DEGREE SHOCK GENERATOR, STATION 3 (X = 27.0 cm)				
		Yaw angle (deg)		
Y (cm)	Z (cm) =	1.57	1.05	0.50
0.25		–2	2	2
0.50		0	1	0
0.75		1	0	–2
1.00		0	–2	–3
1.25		–1	–4	–3
1.50		–3	–4	–4
1.75		–4	–5	–4
2.00		–6	–5	–4
2.25		–7	–5	–4
2.50		–8	–6	–5
2.75		–8	–6	–5
3.00		–9	–6	–4
3.25		–9	–6	–4
3.50		–9	–6	–3
3.75		–10	–6	–2
4.00		–10	–5	–2
4.25		–11	–5	–2
4.50		–12	–6	–3
4.75		–12	–6	–3
5.00		–12	–6	–3
5.25		–12	–6	–3
5.50		–13	–6	–2
5.75		–12	–6	–2
6.00		–12	–6	–2

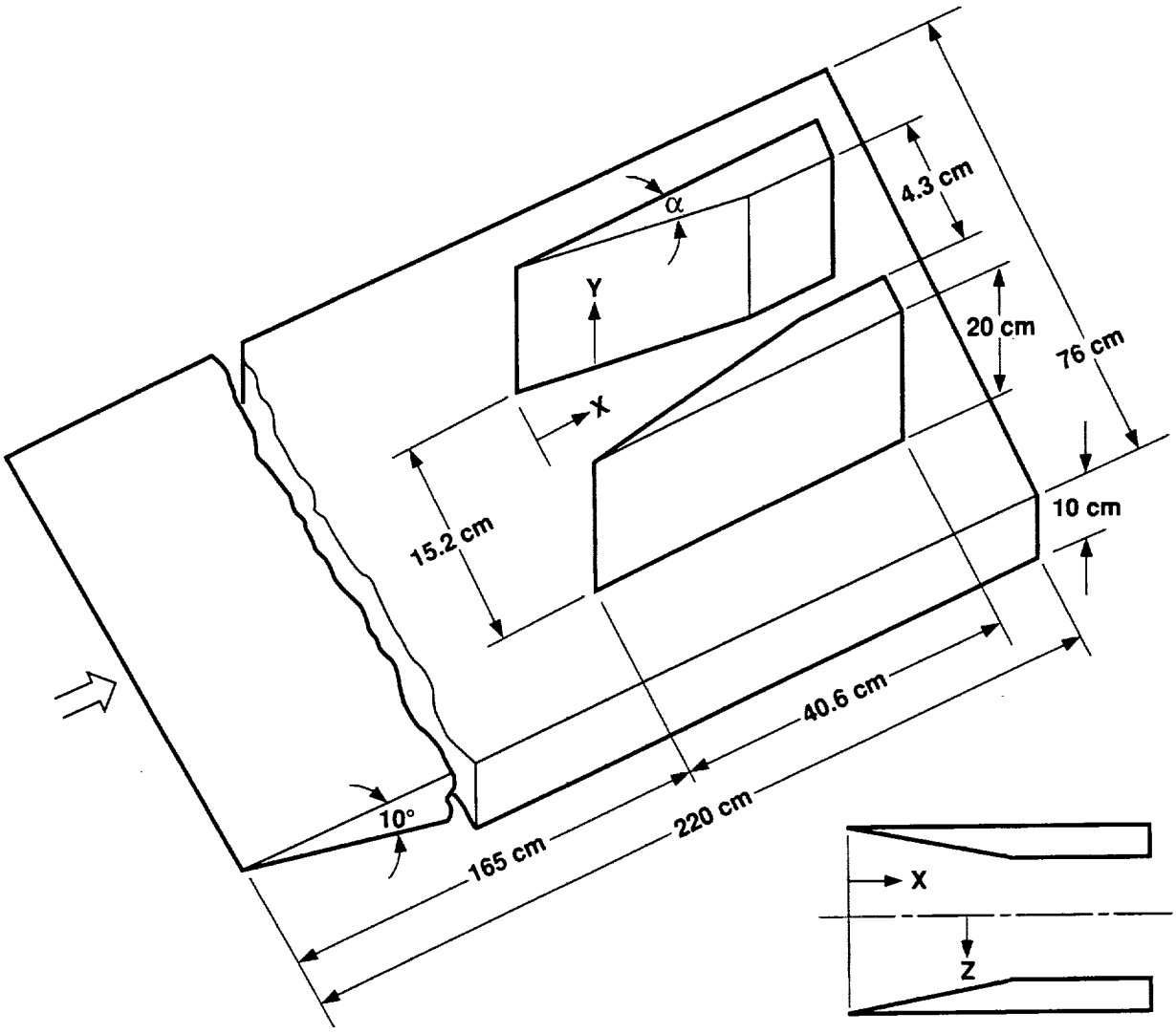

Figure 1. Test-body configuration and coordinate system.

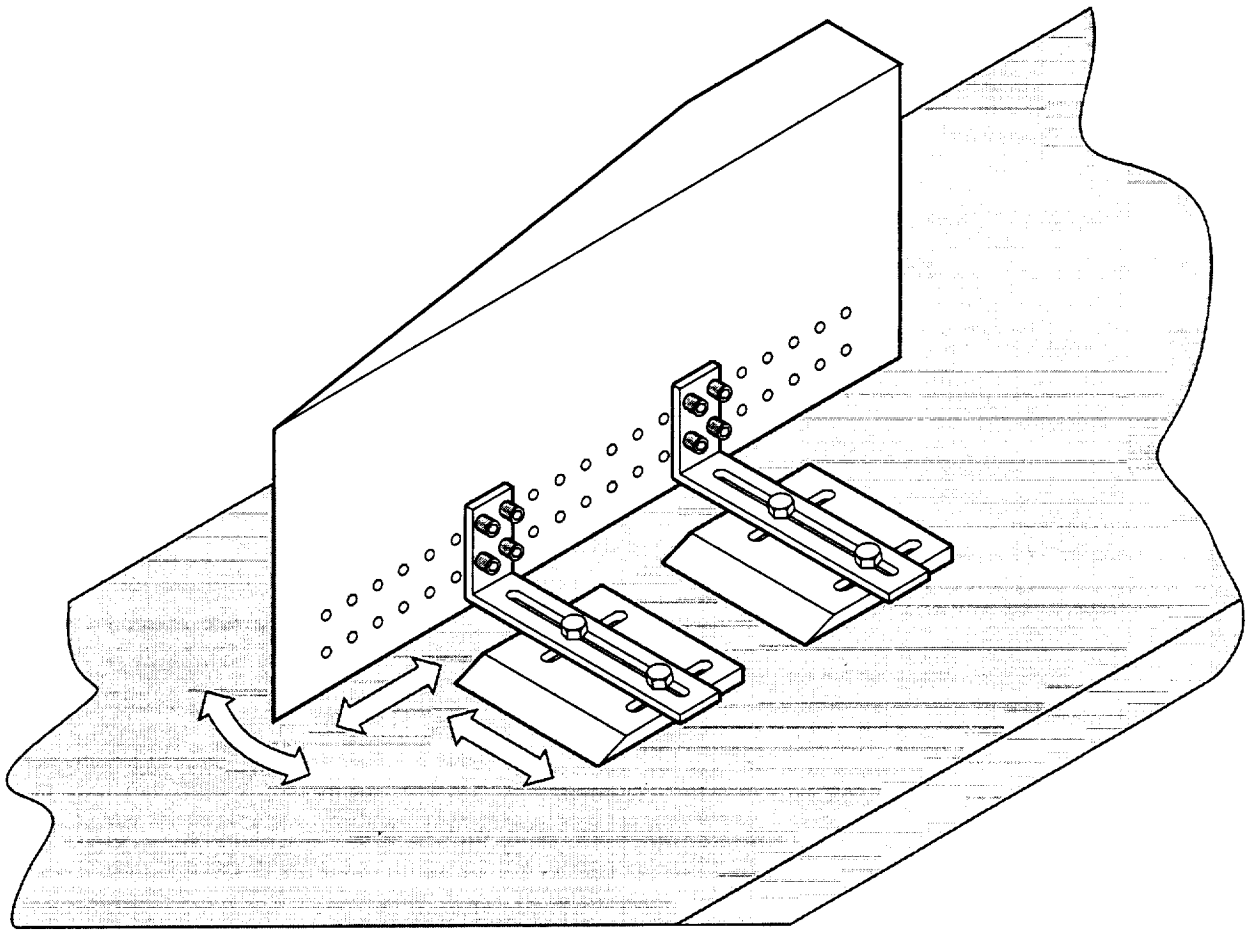

Figure 2. Apparatus for translating double-fin configuration.

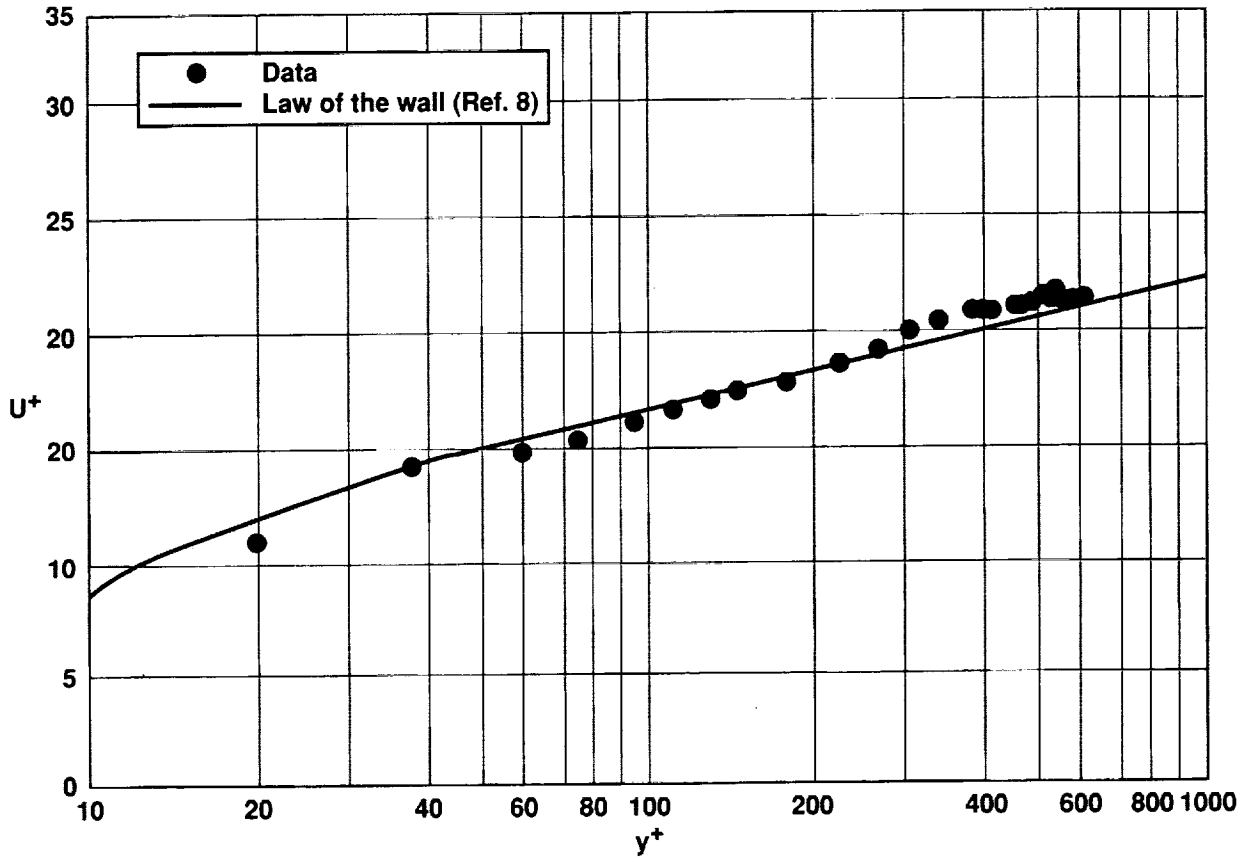

Figure 3. Mean velocity distribution in law-of-the-wall coordinates for the undisturbed boundary layer.

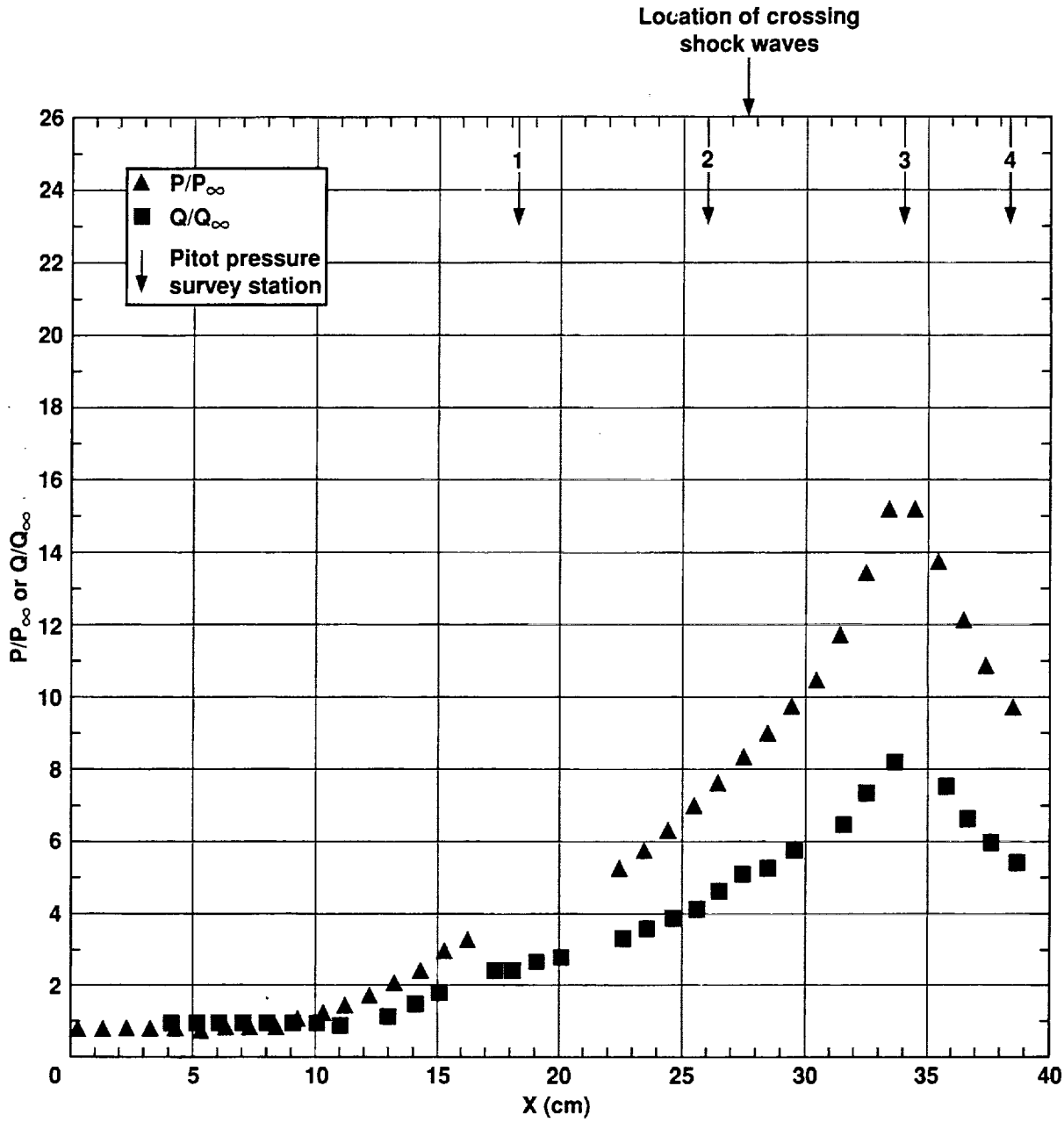

Figure 4. Streamwise varation of pressure and heat transfer on flat-plate surface (y, z = 0 cm), 10° double-fin configuration.

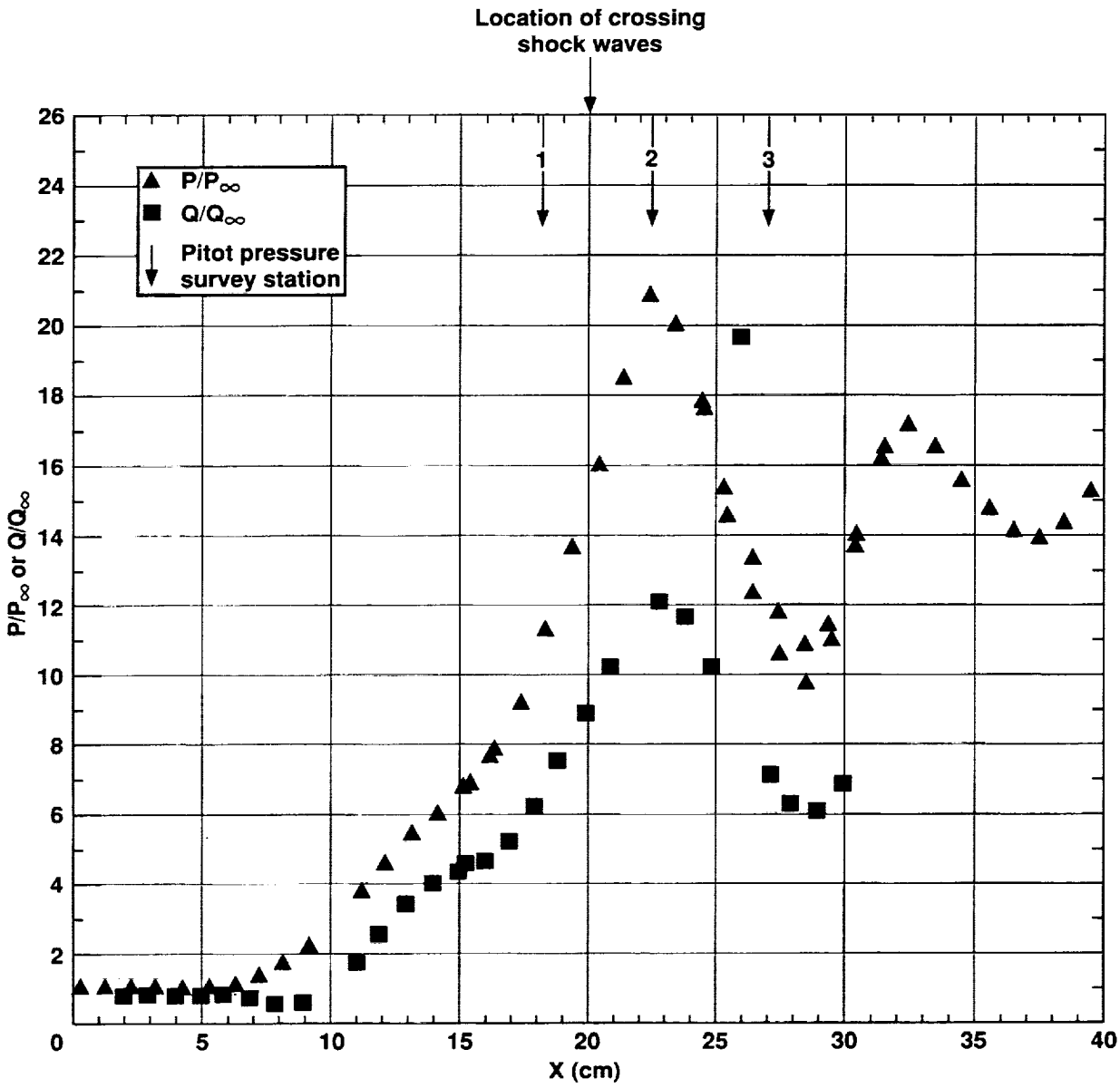

Figure 5. Streamwise varation of pressure and heat transfer on flat-plate surface (y, z = 0 cm), 15° double-fin configuration.

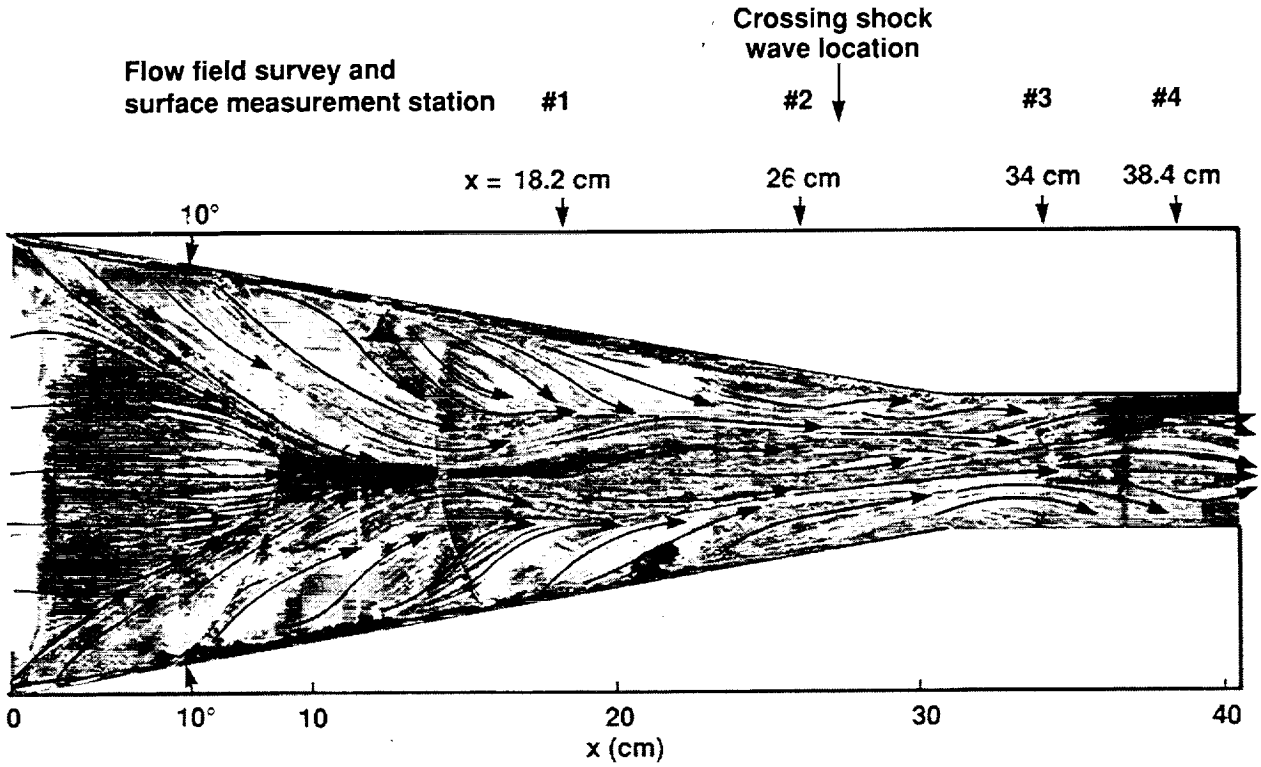

(a) Actual skin friction lines

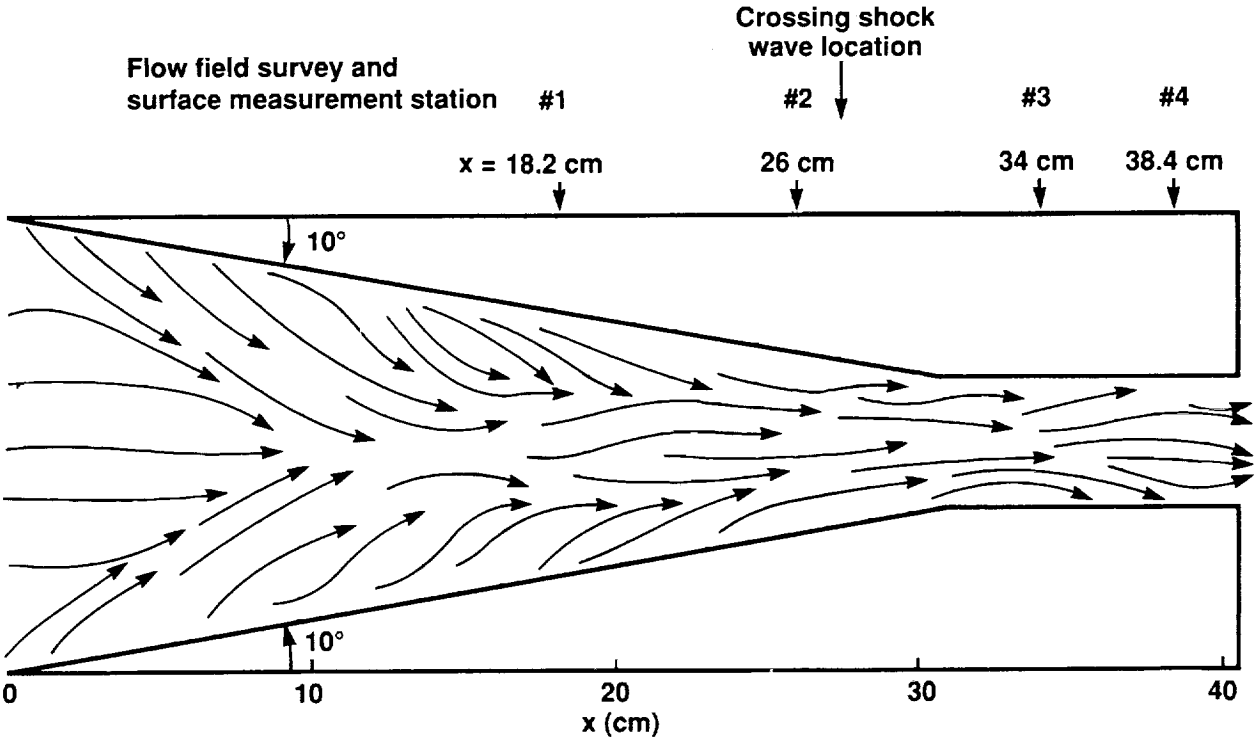

(b) Sketch of surface skin friction lines

Figure 6. Flow visualization, flat-plate surface, 10° double-fin configuration.

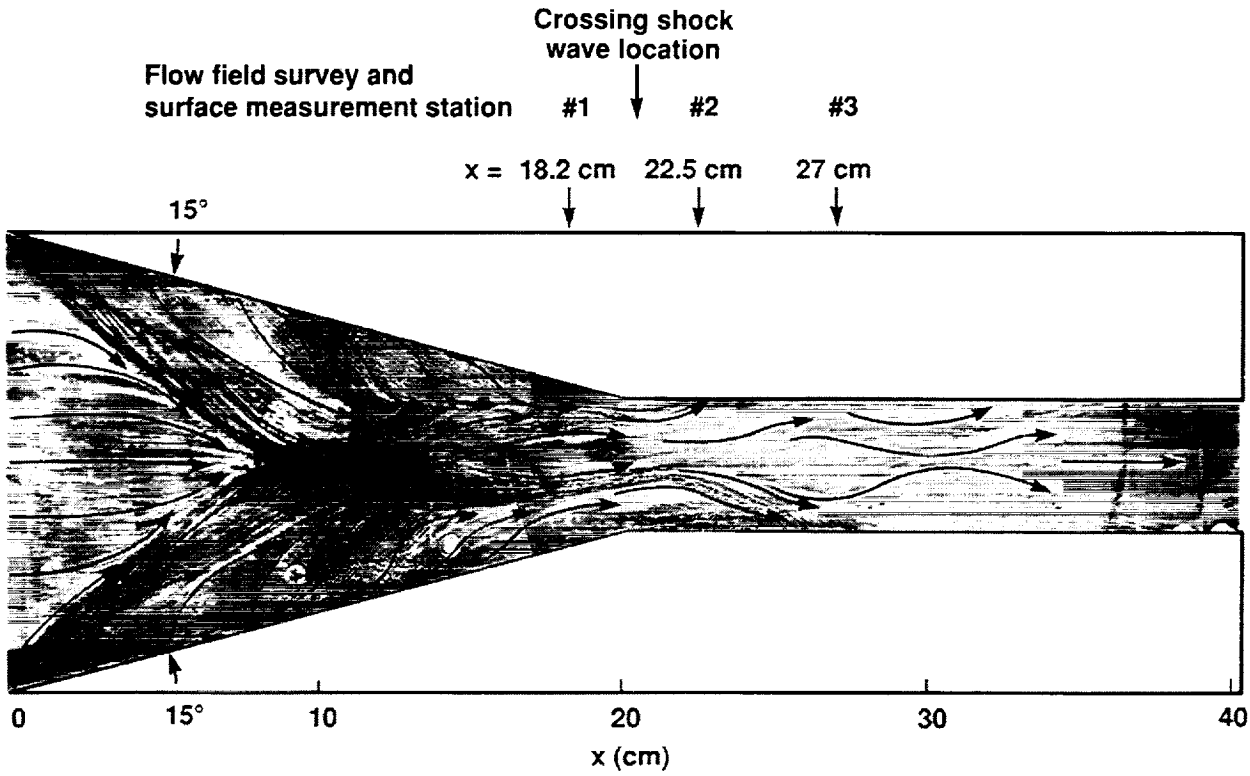

(a) Actual skin friction lines

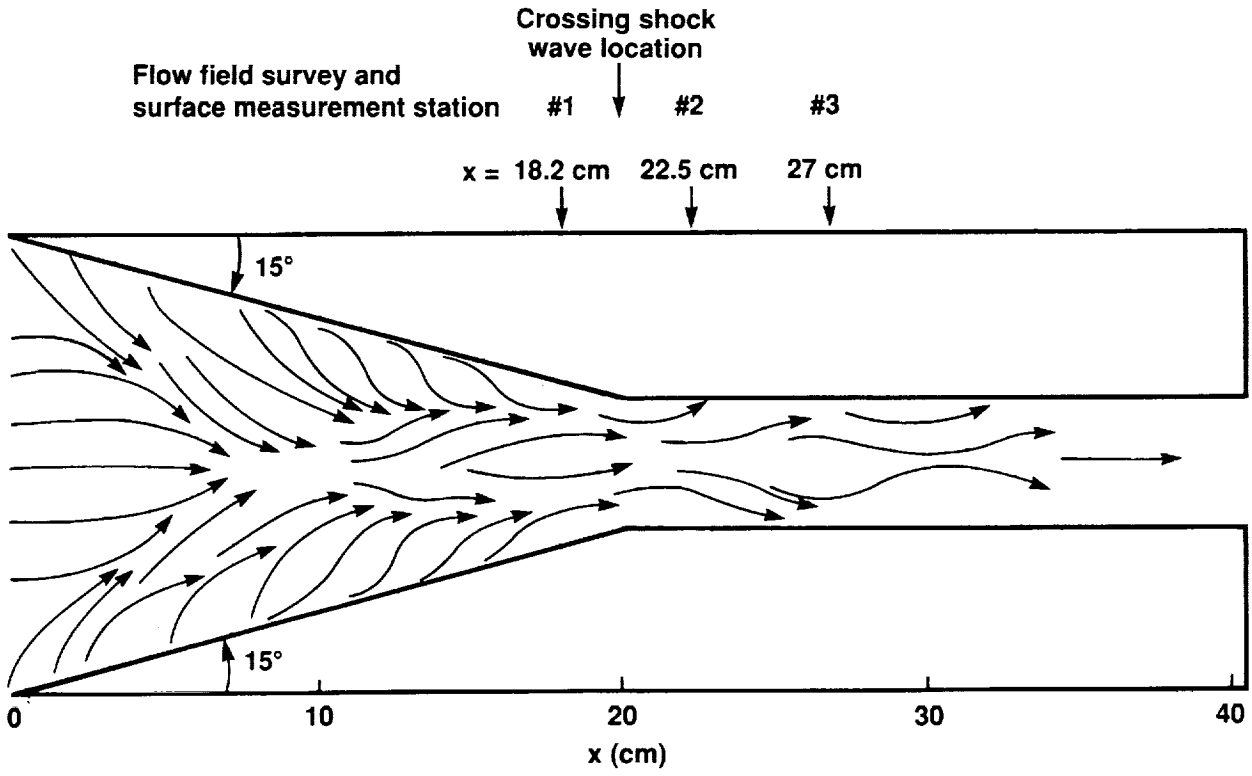

(b) Sketch of surface skin friction lines

Figure 7. Flow visualization, flat-plate surface, 15° double-fin configuration.

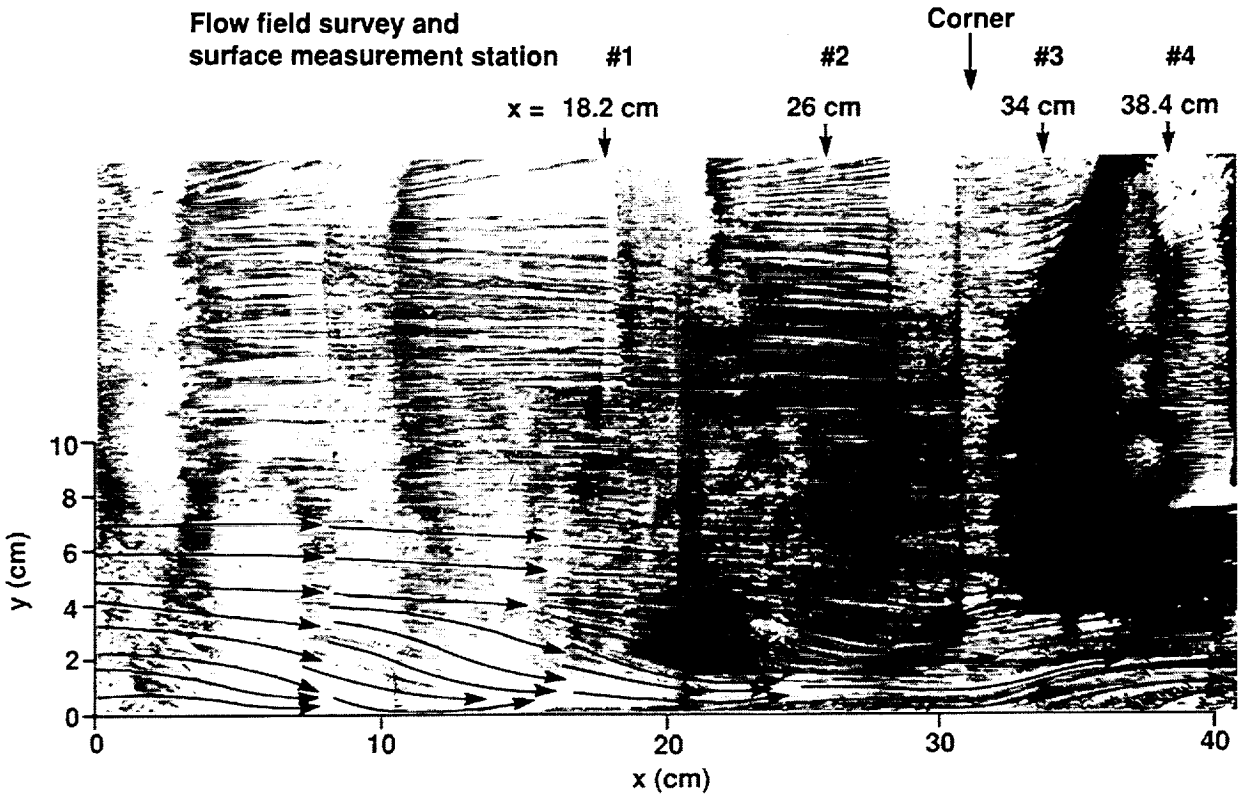

(a) Actual skin friction lines

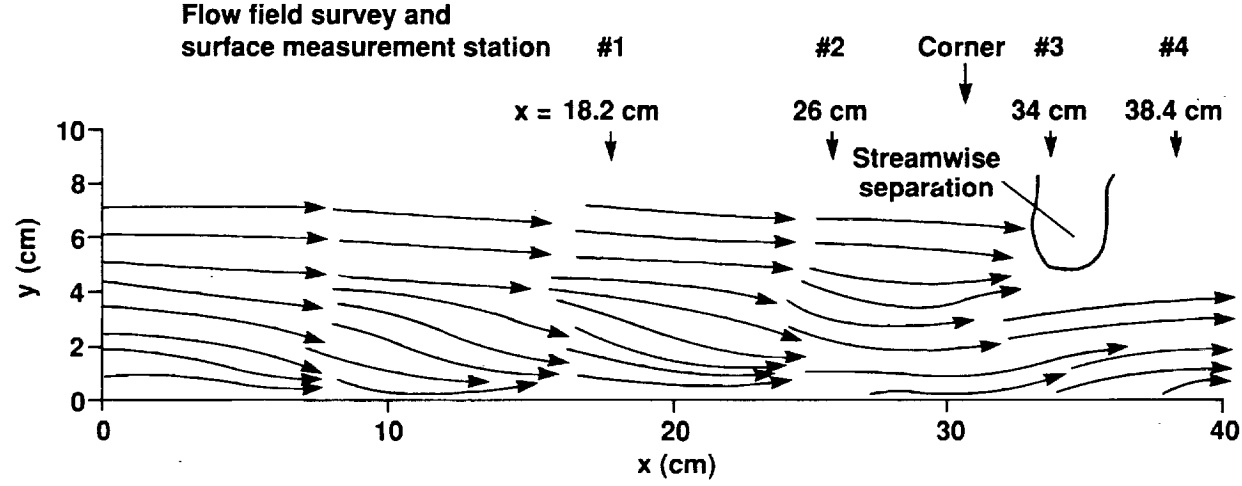

(b) Sketch of surface skin friction lines

Figure 8. Flow visualization, right fin surface, 10° double-fin configuration.

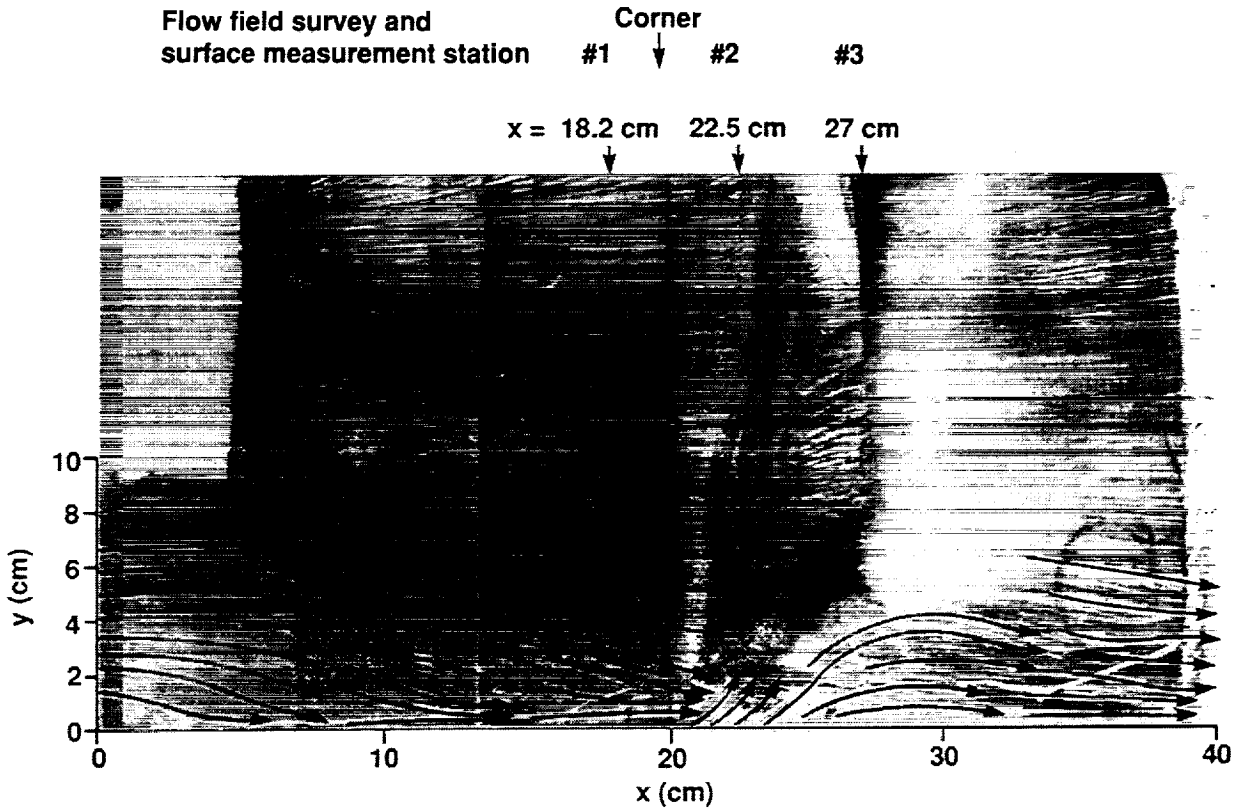

(a) Actual skin friction lines

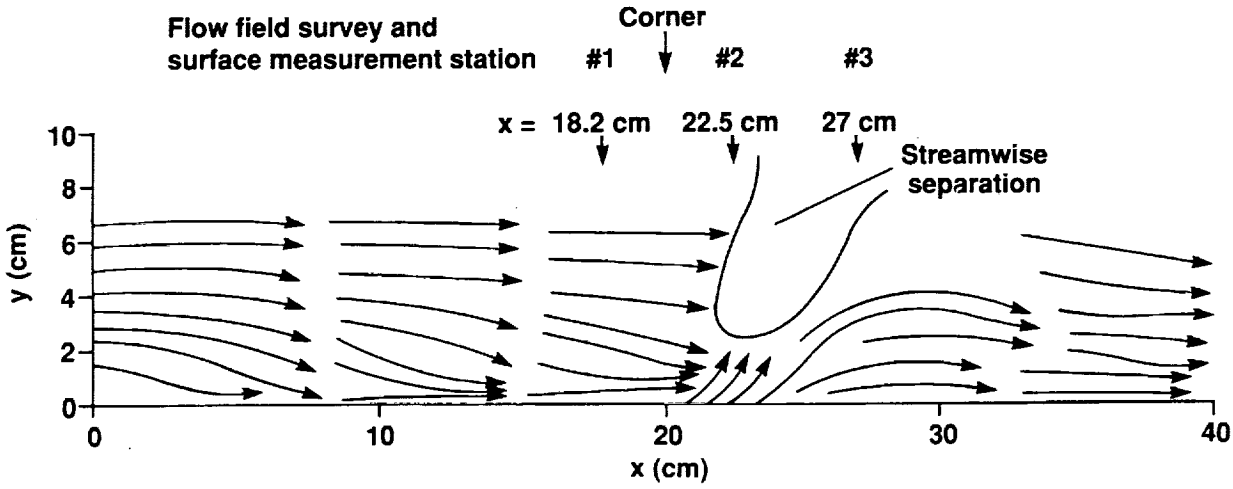

(b) Sketch of surface skin friction lines

Figure 9. Flow visualization, right fin surface, 15° double-fin configuration.

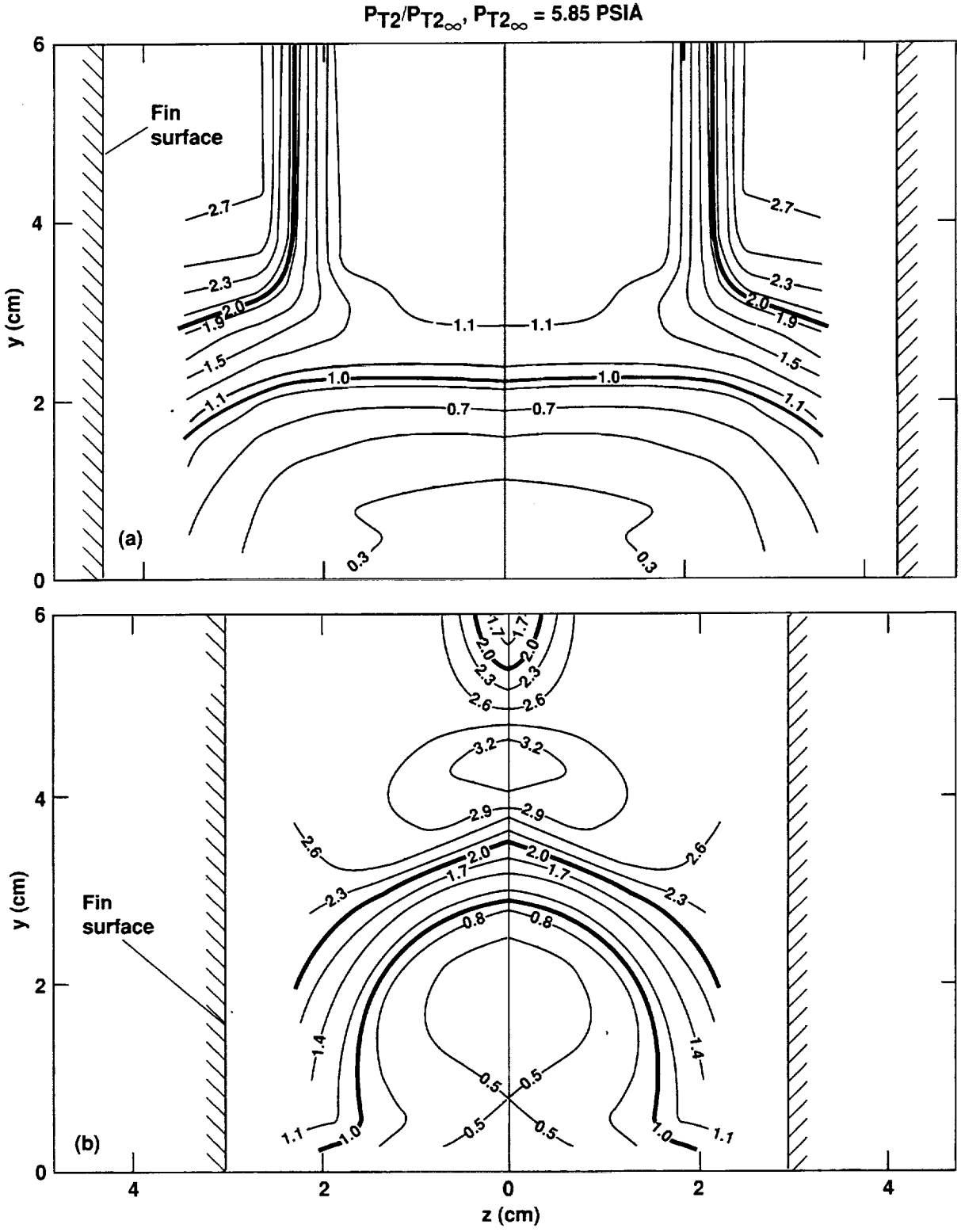

Figure 10. Flow-field pitot pressure contours for the 10° double-fin configuration. (a) Station 1, x = 18.2 cm, (b) station 2, x = 26.0 cm.

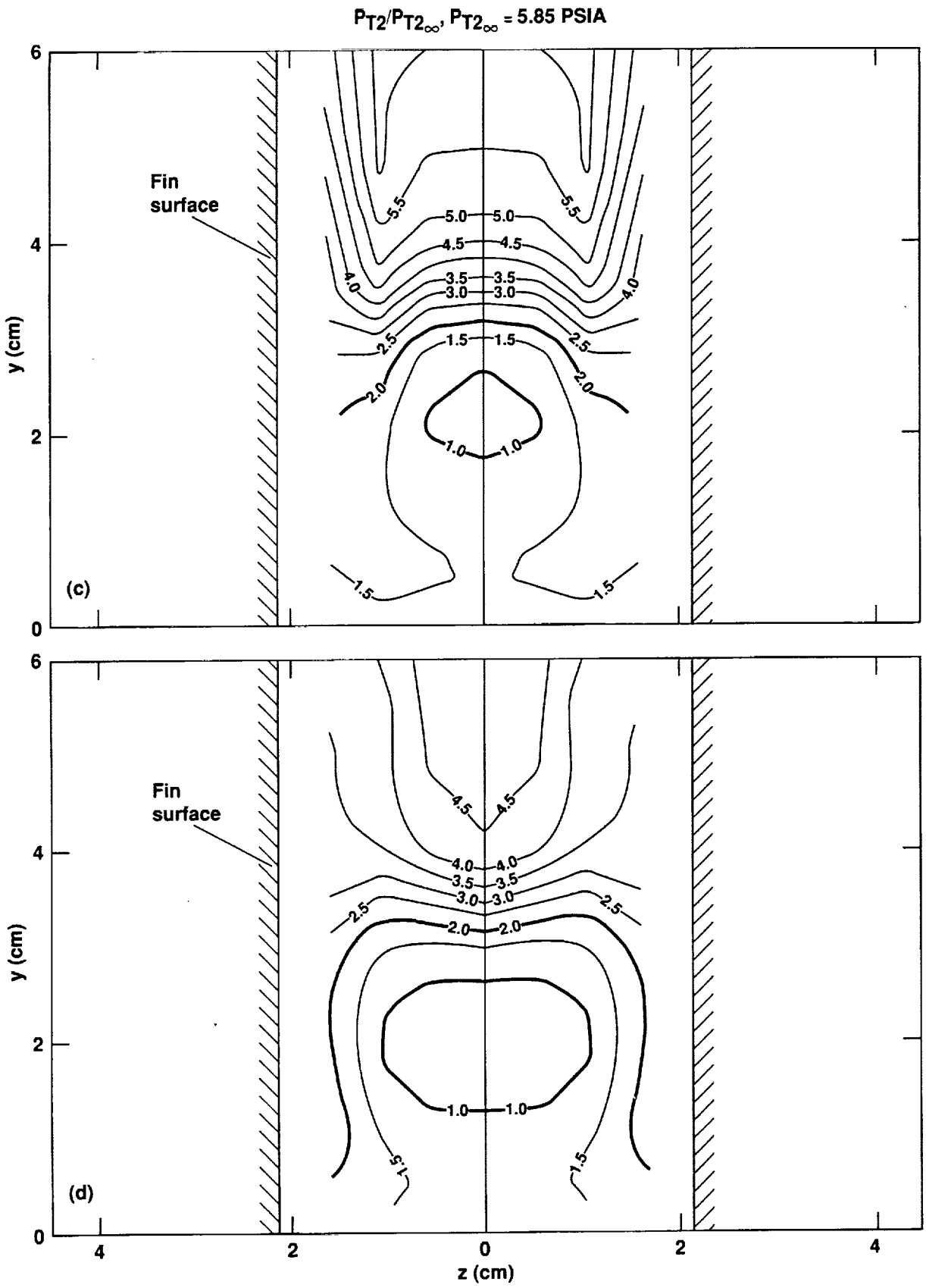

Figure 10. Concluded. (c) Station 3, x = 34.0 cm, (d) station 4, x = 38.3 cm.

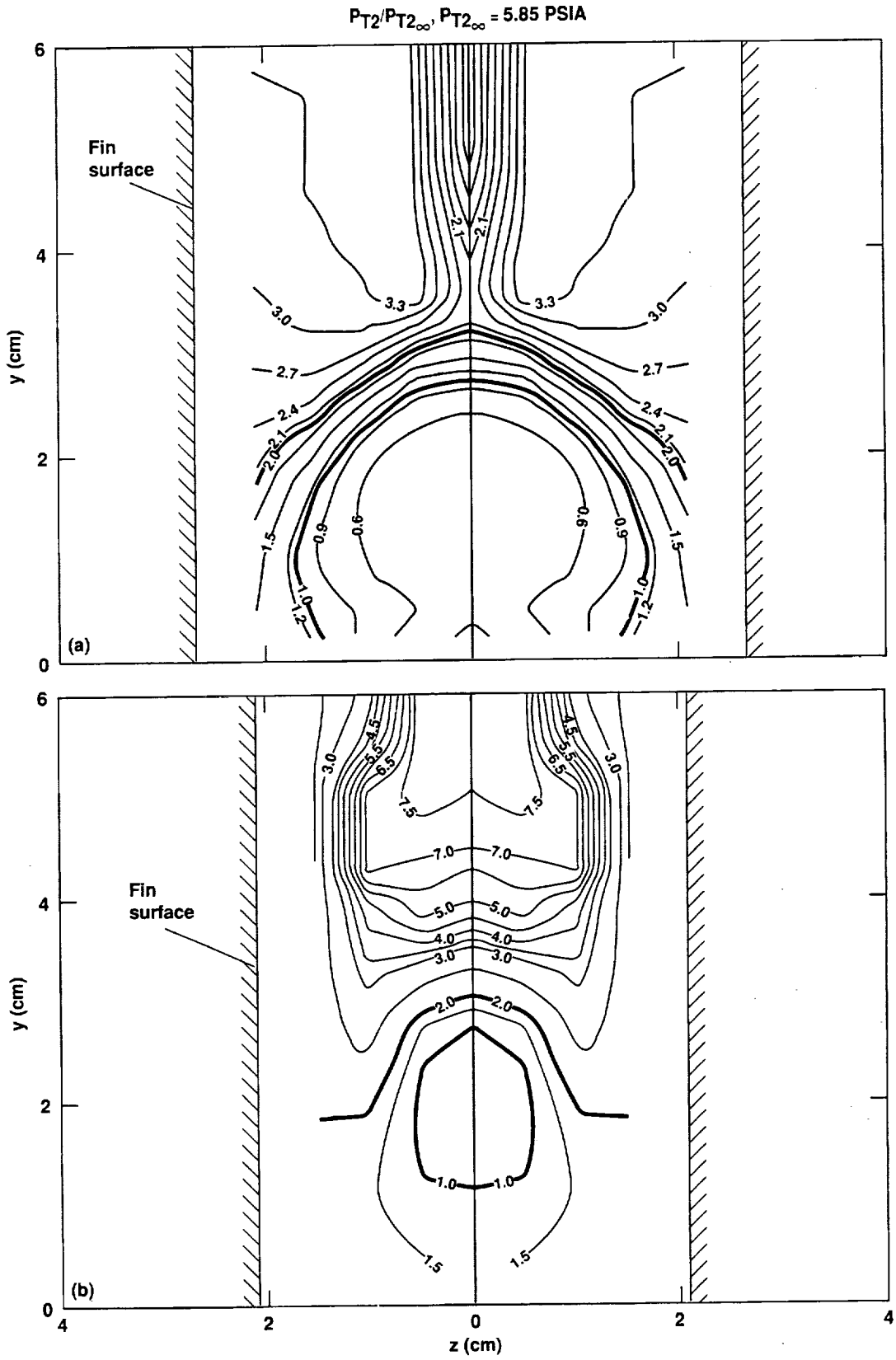

Figure 11. Flow-field pitot pressure contours for the 15° double-fin configuration. (a) Station 1, x = 18.2 cm, (b) station 2, x = 22.5 cm.

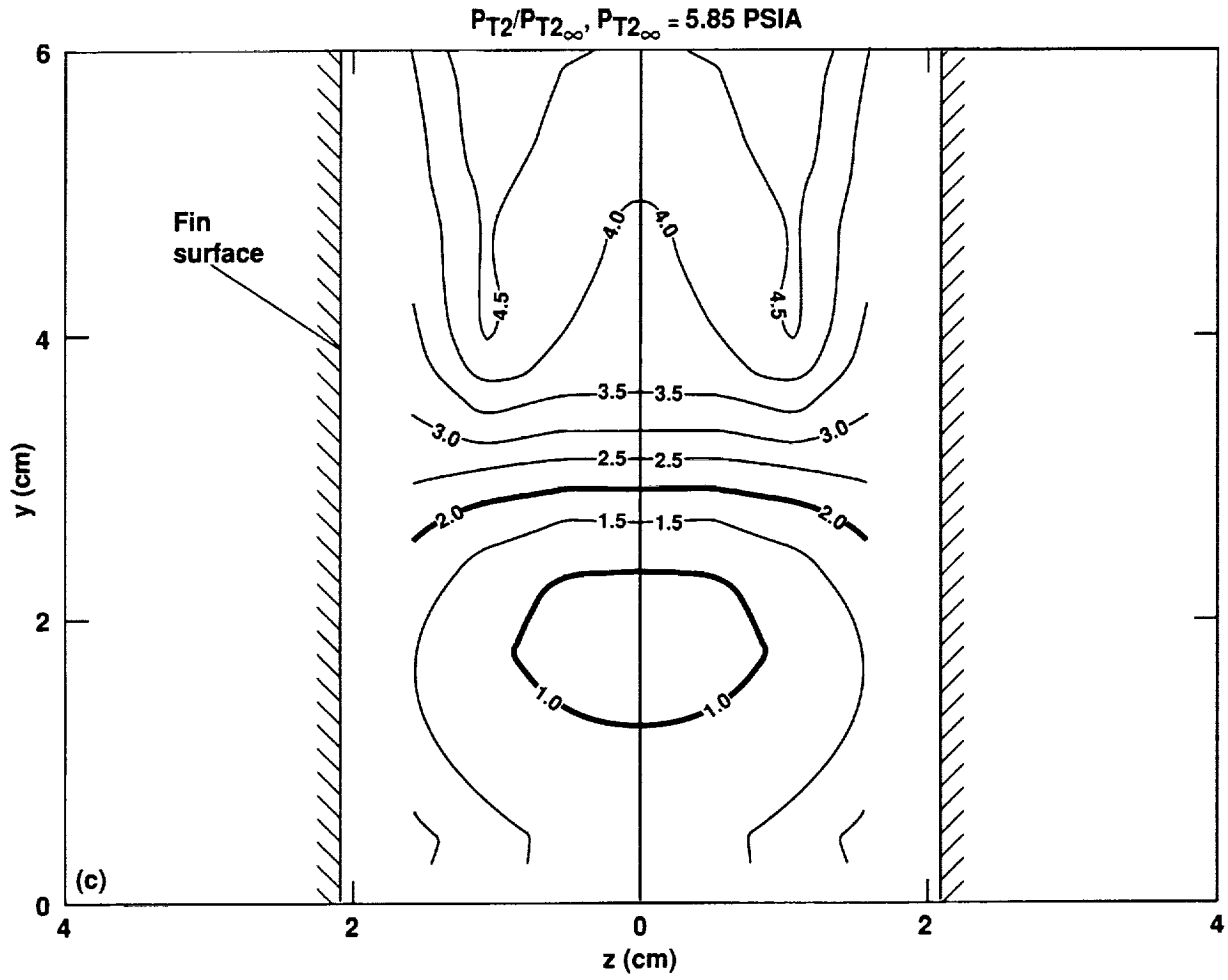

Figure 11. Concluded. (c) Station 3, x = 27.0 cm.

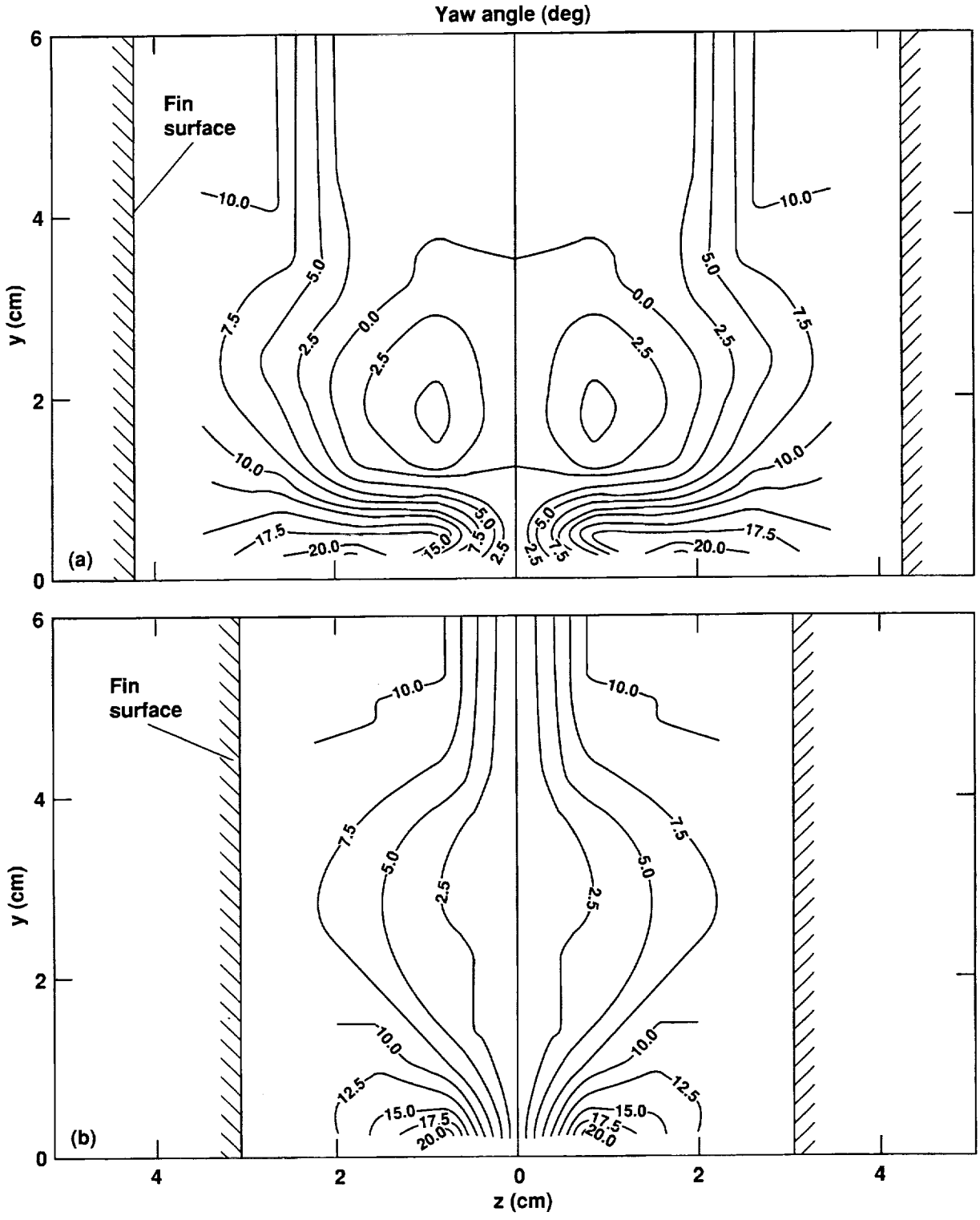

Figure 12. Flow-field yaw angle contours for the 10° double-fin configuration. (a) Station 1, x = 18.2 cm, (b) station 2, x = 26.0 cm.

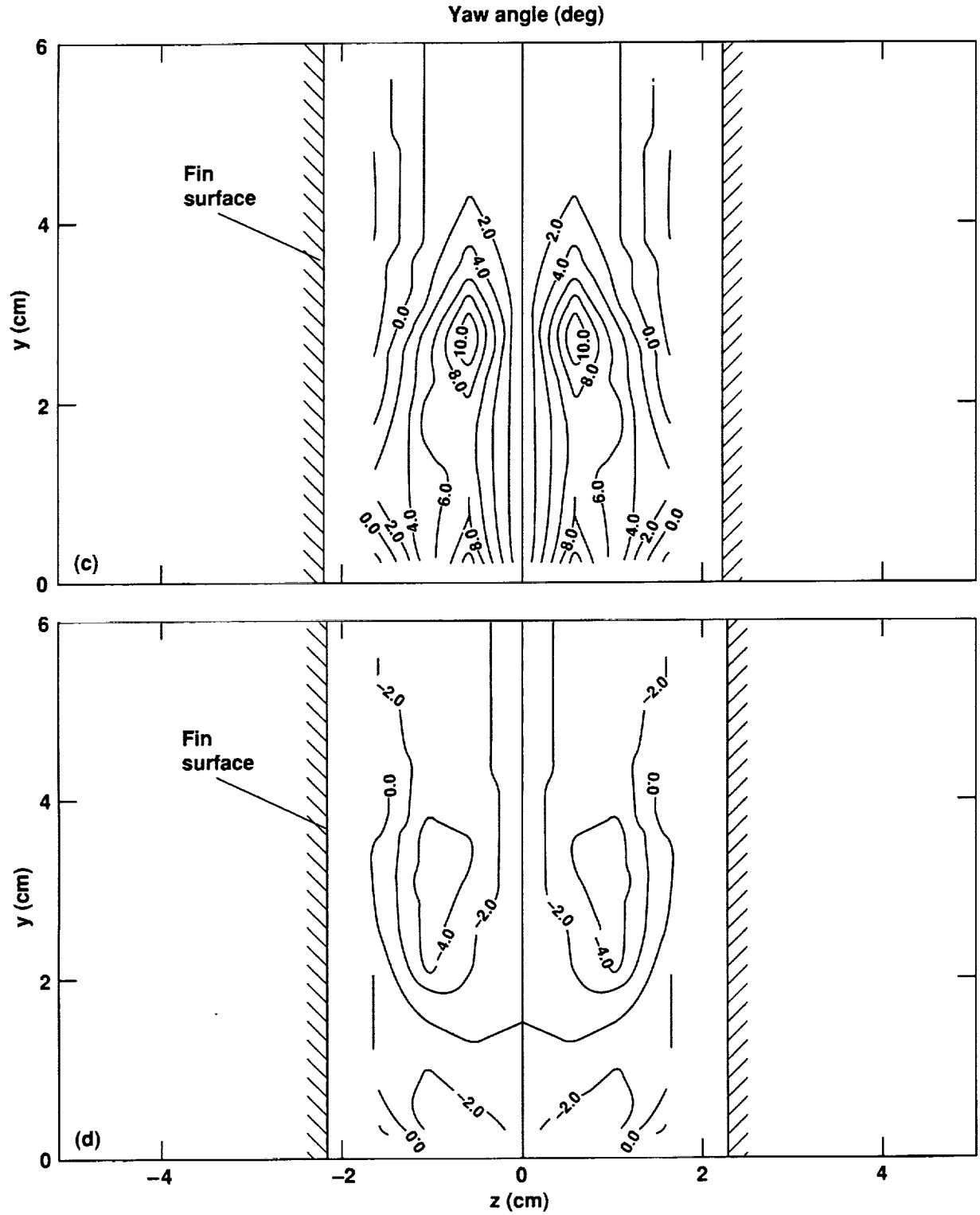

Figure 12. Concluded. (c) Station 3, x = 34.0 cm, (d) station 4, x = 38.3 cm.

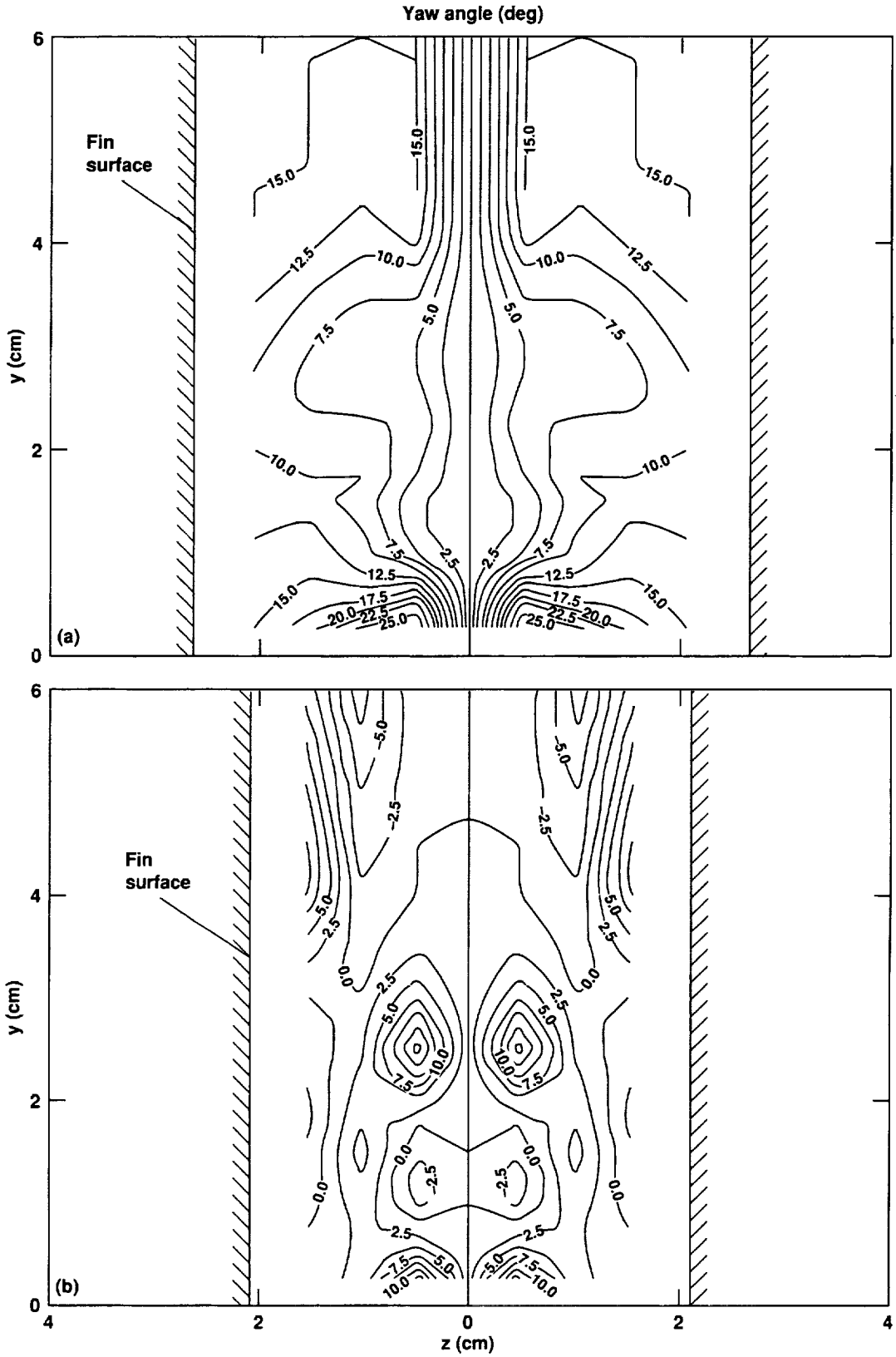

Figure 13. Flow-field yaw angle contours for the 15° double-fin configuration. (a) Station 1, x = 18.2 cm, (b) station 2, x = 22.5 cm.

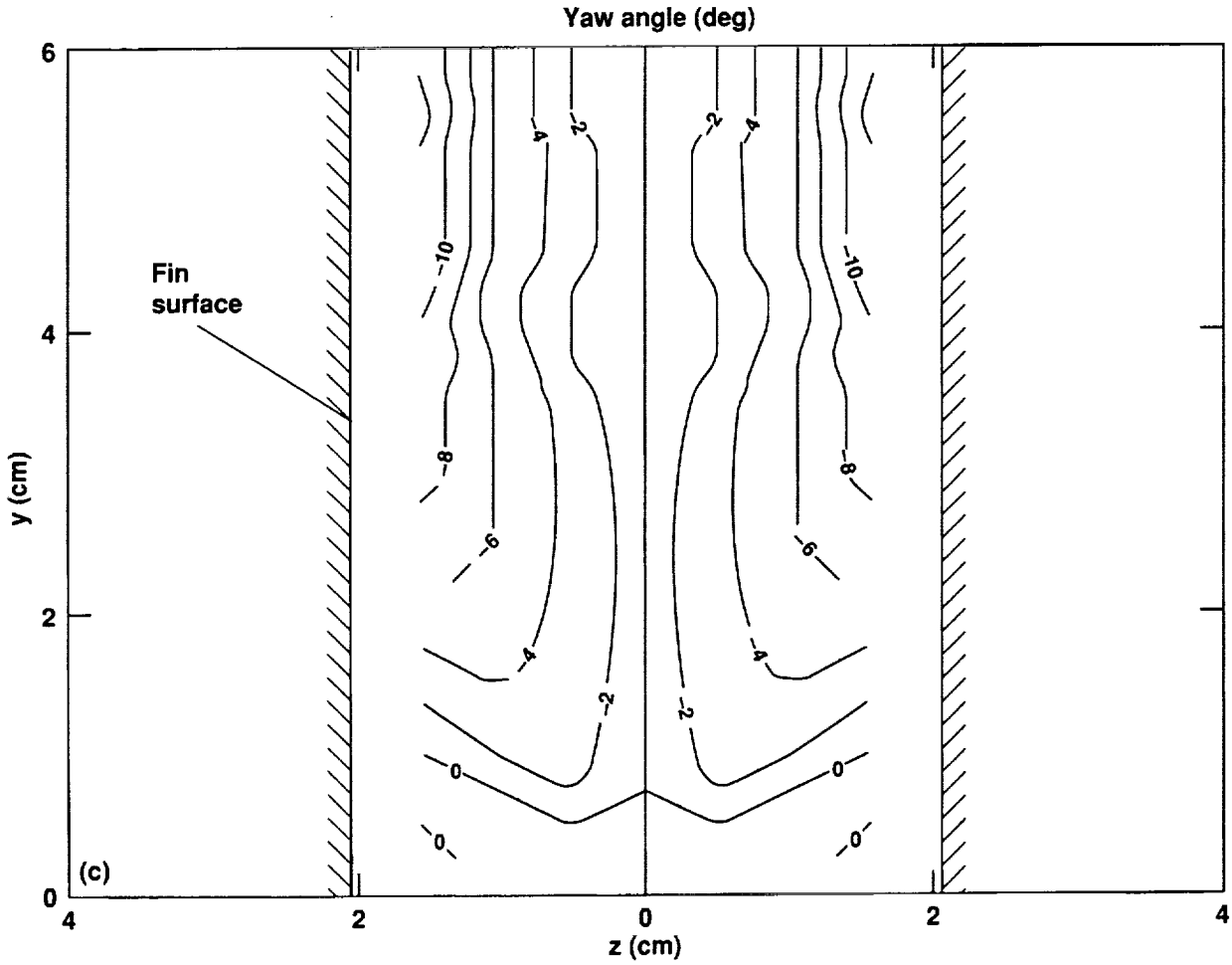

Figure 13. Concluded. (c) Station 3, x = 27.0 cm.

REPORT DOCUMENTATION PAGE

Form Approved
OMB No. 0704-0188

1. AGENCY USE ONLY *(Leave blank)*	2. REPORT DATE	3. REPORT TYPE AND DATES COVERED
	February 1992	Technical Memorandum

4. TITLE AND SUBTITLE

Intersecting Shock-Wave/Turbulent Boundary-Layer Interactions at Mach 8.3

5. FUNDING NUMBERS

505-59-40

6. AUTHOR(S)

M. I. Kussoy* and K. C. Horstman*

7. PERFORMING ORGANIZATION NAME(S) AND ADDRESS(ES)

Ames Research Center
Moffett Field, CA 94035-1000

8. PERFORMING ORGANIZATION REPORT NUMBER

A-92027

9. SPONSORING/MONITORING AGENCY NAME(S) AND ADDRESS(ES)

National Aeronautics and Space Administration
Washington, DC 20546-0001

10. SPONSORING/MONITORING AGENCY REPORT NUMBER

NASA TM-103909

11. SUPPLEMENTARY NOTES

*Eloret Institute, Palo Alto, California.
Point of Contact: M. I. Kussoy, Ames Research Center, MS 229-1, Moffett Field, CA 94035-1000
(415) 604-6192 or FTS 464-6192

12a. DISTRIBUTION/AVAILABILITY STATEMENT

Unclassified — Unlimited
Subject Category 34

12b. DISTRIBUTION CODE

13. ABSTRACT ***(Maximum 200 words)***

Experimental data for two three-dimensional intersecting shock-wave/turbulent boundary-layer interaction flows at Mach 8.3 are presented. The test bodies, composed of two sharp fins fastened to a flat-plate test bed, were designed to generate flows with varying degrees of pressure gradient, boundary-layer separation, and turning angle. The data include surface pressure and heat transfer distributions as well as mean flow-field surveys both in the undisturbed and interaction regimes. The data are presented in a convenient form to be used to validate existing or future computational models of these hypersonic flows. The data are also on a 3.5-inch diskette included with this document, and are available through E-mail. This work was supported by a grant from NASA to Eloret Institute (NCC2-452).

14. SUBJECT TERMS

Shock wave, Turbulent boundary layer, Heat transfer

15. NUMBER OF PAGES

49

16. PRICE CODE

A03

17. SECURITY CLASSIFICATION OF REPORT	18. SECURITY CLASSIFICATION OF THIS PAGE	19. SECURITY CLASSIFICATION OF ABSTRACT	20. LIMITATION OF ABSTRACT
Unclassified	Unclassified		